

EMERGENT THERMODYNAMICS IN A SYSTEM OF MACROSCOPIC, CHAOTIC
SURFACE WAVES

by

KYLE J. WELCH

A DISSERTATION

Presented to the Department of Physics
and the Graduate School of the University of Oregon
in partial fulfillment of the requirements
for the degree of
Doctor of Philosophy

September 2016

DISSERTATION APPROVAL PAGE

Student: Kyle J. Welch

Title: Emergent Thermodynamics in a System of Macroscopic, Chaotic Surface Waves

This dissertation has been accepted and approved in partial fulfillment of the requirements for the Doctor of Philosophy degree in the Department of Physics by:

Raghuveer Parthasarathy

Chair

Eric Corwin

Advisor

Benjamin McMorran

Core Member

Michael Kellman

Institutional Representative

and

Scott L. Pratt

Dean of the Graduate School

Original approval signatures are on file with the University of Oregon Graduate School.

Degree awarded September 2016

© 2016 Kyle J. Welch

This work is licensed under a Creative Commons

Attribution-NonCommercial-NoDerivs (United States) License.



DISSERTATION ABSTRACT

Kyle J. Welch

Doctor of Philosophy

Department of Physics

September 2016

Title: Emergent Thermodynamics in a System of Macroscopic, Chaotic Surface Waves

The properties of conventional materials are inextricably linked with their molecular composition; to make water flow like wine would require changing its molecular identity. To circumvent this restriction, I have constructed and characterized a two-dimensional *metafluid*, so-called because its constitutive dynamics are derived not from atoms and molecules but from macroscopic, chaotic surface waves excited on a vertically agitated fluid. Unlike in conventional fluids, the viscosity and temperature of this metafluid are independently tunable. Despite this unconventional property, our system is surprisingly consistent with equilibrium thermodynamics, despite being constructed from macroscopic, non-equilibrium elements. As a programmable material, our metafluid represents a new platform on which to study complex phenomena such as self-assembly and pattern formation. We demonstrate one such application in our study of short-chain polymer analogs embedded in our system.

Chapter 2 has been published in *Physical Review E* [15]. The writing and analysis were performed by me as primary author. Eric Corwin is listed as a coauthor as he advised this work. The material in this chapter is also co-authored with Raghuvveer Parthasarathy, for use of his image analysis software and contributions to the early design and motivation of the experiment, and Isaac Hastings-Hauss, an undergraduate who helped with construction of the system.

Chapter 4 has also been published in *Physical Review E* [16]. The writing and analysis were performed by me as primary author. Eric Corwin is listed as a coauthor as he advised this work. The material in this chapter is also coauthored with Clayton Kilmer, an undergraduate who helped with data collection. At the time of this writing, chapter 3 has been accepted to *Proceedings of the National Academy of Sciences* but is not yet in print. The writing and analysis were performed by me as primary author. Eric Corwin is listed as a coauthor as he

advised this work. The material in this chapter is also coauthored with Alex Liebman-Peláez, an undergraduate who helped with construction of parts of the experimental system.

This dissertation includes previously published and unpublished co-authored material.

CURRICULUM VITAE

NAME OF AUTHOR: Kyle J. Welch

GRADUATE AND UNDERGRADUATE SCHOOLS ATTENDED:

University of Oregon, Eugene, OR
Washington State University, Pullman, WA

DEGREES AWARDED:

Doctor of Philosophy, Physics, 2016, University of Oregon
Bachelor of Science, Physics, *magna cum laude*, 2011, Washington State University
Bachelor of Science, Neuroscience, *magna cum laude*, 2011, Washington State University

AREAS OF SPECIAL INTEREST:

Soft Condensed Matter, Non-equilibrium Physics, Biophysics

PROFESSIONAL EXPERIENCE:

Research Assistant, Physics, University of Oregon, 2012-2016
Teaching Assistant, Physics, University of Oregon, 2011-2012, 2015, 2016
Teaching Assistant, Chemistry, Washington State University, 2008-2011

GRANTS, AWARDS AND HONORS:

Weiser Senior Teaching Assistant Award, University of Oregon, 2015
Weiser First Year Teaching Assistant Award, University of Oregon, 2012
Regents Scholar, Washington State University, 2006-2011

PUBLICATIONS:

K. J. Welch, A. Liebman-Pelaez, E. I. Corwin. "Chaotic surface waves form a metafluid that is Newtonian, thermal and entirely tunable." *Proceedings of the National Academy of Science* (accepted).

K. J. Welch, C. S. G. Kilmer, E. I. Corwin. "Atomistic study of macroscopic analogs to short chain molecules." *Physical Review E*, **91**, 022603 (2015).

K. J. Welch, I. Hastings-Hauss, E. I. Corwin. "Ballistic and diffusive dynamics in a two-dimensional ideal gas of macroscopic chaotic Faraday waves." *Physical Review E*, **89**, 042143 (2014).

ACKNOWLEDGEMENTS

All of this work has been done under the guidance of my graduate advisor, Eric Corwin, who has taught me a great deal about science, the academic process, and life in general. I would also like to thank Raghu Parthasarathy for his guidance, mentoring and honest feedback on paper manuscripts and presentations throughout my time as a graduate student. For helpful discussions, I would like to thank John Royer and John Toner. Olivia Carey-De La Torre and Cody Hill provided initial machine work on the large dish used for the work presented in chapters 3 and 4. This work was primarily funded by the NSF under Career Award No. DMR-1255370. ALP (co-author on chapter 3) was supported under the Research Experience for Undergraduates program sponsored by the UO Materials Science Institute and the NSF.

TABLE OF CONTENTS

| Chapter | | Page |
|---------|--|------|
| I. | INTRODUCTION | 1 |
| II. | BALLISTIC AND DIFFUSIVE DYNAMICS IN A TWO-DIMENSIONAL IDEAL GAS OF MACROSCOPIC CHAOTIC FARADAY WAVES | 4 |
| | Abstract | 4 |
| | Background | 4 |
| | Methods | 6 |
| | Results and Discussion | 9 |
| | Conclusion | 14 |
| III. | FLUIDS BY DESIGN: CHAOTIC SURFACE WAVES FORM A METAFUID THAT IS NEWTONIAN, THERMAL AND ENTIRELY TUNABLE | 15 |
| | Abstract | 15 |
| | Background | 15 |
| | Results and Discussion | 17 |
| | Conclusion | 25 |
| IV. | ATOMISTIC STUDY OF MACROSCOPIC ANALOGS TO SHORT CHAIN MOLECULES | 26 |
| | Abstract | 26 |
| | Background | 26 |
| | Materials and Methods | 27 |
| | Data Analysis and Simulation | 29 |
| | Conclusion | 36 |

| Chapter | Page |
|--|------|
| V. DETAILED MATERIALS AND METHODS FOR CHAPTER 3 | 38 |
| Shaker Assembly | 38 |
| Rheometer | 38 |
| Derivation of Torque Due to Magnets | 39 |
| Measurement of Drag Coefficient | 40 |
| VI. SUPPLEMENTARY MATERIALS FOR CHAPTER 4 | 44 |
| Effective Potentials for Chain With $\alpha = \pi/6$ | 44 |
| Semiflexible Behavior | 46 |
| Self avoiding walk simulation algorithm | 46 |
| VII. CONCLUSION | 47 |
| REFERENCES CITED | 52 |

LIST OF FIGURES

| Figure | Page |
|--|------|
| 1. Experimental Apparatus | 7 |
| 2. Map of parameter space. | 8 |
| 3. Ballistic and Diffusive Behavior | 10 |
| 4. Gas behavior | 13 |
| 5. Experimental setup and Characterization | 16 |
| 6. Tunable Newtonian Fluid Behavior | 19 |
| 7. Einstein Relation and Green-Kubo Relation | 22 |
| 8. Phase Space and Parameter Space | 24 |
| 9. Experimental Design | 28 |
| 10. Pair Correlation Function | 31 |
| 11. Effective Potentials | 32 |
| 12. Master curves for the scaling of winding angle variance σ_ϕ^2 | 34 |
| 13. Scaling Laws for End-to-End Distance | 36 |
| 14. Comparison of Hookean approximation and full form for torque exerted by drive arm | 41 |
| 15. Effective Potentials in Total Bond Winding Angle $\phi_{i,j}$ | 44 |
| 16. Effective potentials for interparticle distance $r_{i,j+1}$ | 45 |
| 17. Extrapolated Effective Potentials for End-to-End distance of Long Chains | 46 |

CHAPTER I

INTRODUCTION

Materials science is a lot like cooking. We do our best to understand the properties of the ingredients, then manipulate and combine them to create new, hopefully useful (or delicious) substances. However, in cooking we are ultimately limited by the properties of our ingredients; no matter how hard we try we can't make pot roast out of a watermelon. Materials science seeks to overcome the limitation of its ingredients by not only understanding, but directly controlling the properties of matter. To do so, however, one must surmount the nearly impossible task of dynamically manipulating the molecular nature of the material, because like a cake, the properties of a conventional material are ultimately defined by the properties of its ingredients. For example, you can tell the difference between water and corn syrup simply by watching them flow: corn syrup has a much higher viscosity than water. To make water flow like corn syrup, however, you would need to change the mass and interaction forces of the water molecules, or, put more plainly, you would need to change the very molecular identity of the water, thus transforming one fluid into the other. Such alchemy is beyond the scope of modern science.

What's more, in conventional materials, there exist strict (though often complicated) relationships between material properties. In the case of fluids, for example, there are well-defined laws that relate temperature and viscosity. This means that you cannot change the temperature of a fluid without inducing a commensurate change in the viscosity, as is apparent when one microwaves honey to make it easier to pour. This restriction represents a serious limitation toward attaining full control of the properties of matter as it means that a given fluid can only explore certain combinations of temperature and viscosity. Again, in order to break this limitation, one would need to achieve independent control over the molecular properties of the system. Thus, the challenge of finding or creating truly programmable matter remains an active and exciting area of study.

Recent work is tackling this challenge by creating *metamaterials*: constructed materials that reject the molecule as the fundamental unit and instead substitute some athermal, macroscopic structural element, achieving novel optical [1–3], acoustic [4–6], mechanical, [7–9] and fluid properties [10, 11] that would otherwise be impossible. Remarkable though this

progress is, it comes at a cost. These materials, by deriving their properties from macroscopic, non-equilibrium or anisotropic elements, abandon the physics of equilibrium thermal systems. This means sacrificing a large body of tools that can be used to characterize and understand their behavior. It also leads to a loss of universality; each metamaterial is governed by different physics, and each must be circumstantially re-characterized to establish their governing laws.

My research has instead taken a bottom-up approach to the creation of programmable matter. Whereas the existing body of work surrounding metamaterials focuses on careful, top-down design of constitutive structures, my work instead seeks first to create a meta-system that obeys the barest criteria of equilibrium thermodynamics, then to study the emergent properties of said system. In particular, I have created and characterized a metafluid whose properties are derived from macroscopic chaotic waves excited on the surface of water, independent from the water itself. These waves (known as chaotic Faraday waves [12, 13]) arise on the surface of a fluid when it is vertically agitated above some critical amplitude. They provide isotropic, “molecular” chaos (where the “molecules” here are the waves themselves) and thus satisfy the basic requirements of kinetic theory as outlined by Boltzmann [14]. By embedding buoyant tracers in the waves, I can measure the basic properties of the metafluid: temperature, diffusion constant and viscous drag coefficient. These properties turn out to be identical in nature, but completely divorced in origin from the analogous properties in conventional fluids. They are associated with the chaos of the waves in the same way that the temperature of a gas is associated with the random motion of its molecules, yet they differ only in scale from their conventional counterparts. As a dramatic comparison, for example, calculations of the ambient thermal energy associated with the chaos of the waves suggests that the metafluid has a characteristic temperature one trillion times hotter than the sun’s surface. This may seem like a ridiculous and specious comparison, but it is made more reasonable when you consider that the sun is largely composed of hydrogen atoms with mass approximately 1.7×10^{-27} kg, whereas the tracer particles thermalized by the chaotic waves have a mass of a few hundred milligrams (10^{-4} kg).

This system carries with it great utility. It constitutes a truly thermal environment while also exhibiting its “molecular” dynamics at the easy-to-access laboratory scale. This means that macroscopic analogs to complicated microscopic phenomena can be studied in atomistic fashion, observing and building up the dynamics from the smallest subunit to the gross bulk behavior.

I have demonstrated one such application in my study of scaling laws in short-chain polymer analogs thermalized by the chaotic surface waves.

In a more far-reaching sense, this research hints at a broader universality of thermodynamics. That all that was required to reproduce equilibrium thermal physics was isotropic chaos suggests that the tools of thermodynamics may be applied to any system that satisfies the basic criteria of kinetic theory. This may include such systems as turbulent weather, bird flocks or complex financial markets.

This work shows that chaotic surface waves form a metafluid that is wholly consistent with equilibrium thermodynamics, despite being composed of macroscopic, non-equilibrium elements. Further, the viscosity and temperature of this metafluid are *independently* tunable. Chapter 2 begins the characterization of this system by examining the motion of passive tracer particles embedded in the chaotic waves, measuring temperature and diffusion constant and how they depend on experimental parameters. Chapter 3 expands this characterization by introducing active rheology to directly measure viscous drag and showing that it, along with temperature and diffusion constant, obeys equilibrium thermodynamics. Chapter 3 also shows, in detail, the dependence of temperature and viscous drag on experimental inputs, and demonstrates that they can be tuned independently of one another. Chapter 4 then illustrates the utility of this system as a novel platform on which complex phenomena may be studied, in this case, the structural dynamics of short-chain polymers analogs.

Chapter 2 has been published in *Physical Review E* [15]. The writing and analysis were performed by me as primary author. Eric Corwin is listed as a coauthor as he advised this work. The material in this chapter is also co-authored with Raghuvveer Parthasarathy, for use of his image analysis software and contributions to the early design and motivation of the experiment, and Isaac Hastings-Hauss, and undergraduate who helped with construction of the system.

Chapter 4 has also been published in *Physical Review E* [16]. The writing and analysis were performed by me as primary author. Eric Corwin is listed as a coauthor as he advised this work. The material in this chapter is also coauthored with Clayton Kilmer, an undergraduate who helped with data collection.

At the time of this writing, chapter 3 has been accepted to *Proceedings of the National Academy of Sciences* but is not yet in print. The writing and analysis were performed by me

as primary author. Eric Corwin is listed as a coauthor as he advised this work. The material in this chapter is also coauthored with Alex Liebman-Peláez, an undergraduate who helped with construction of parts of the experimental system.

CHAPTER II

BALLISTIC AND DIFFUSIVE DYNAMICS IN A TWO-DIMENSIONAL IDEAL GAS OF MACROSCOPIC CHAOTIC FARADAY WAVES

Abstract

We have constructed a macroscopic driven system of chaotic Faraday waves whose statistical mechanics, we find, are surprisingly simple, mimicking those of a thermal gas. We use real-time tracking of a single floating probe, energy equipartition, and the Einstein relation to define and measure a temperature and diffusion constant, and then self-consistently determine a coefficient of viscous friction for a test particle in this thermal-like gas. Because of its simplicity, this system can serve as a model for direct experimental investigation of non-equilibrium statistical mechanics, much as the ideal gas epitomizes equilibrium statistical mechanics.

This work was originally published in *Physical Review E* [15]. The writing and analysis were performed by me as primary author. Eric Corwin is listed as a coauthor as he advised this work. The material in this chapter is also co-authored with Raghuvveer Parthasarathy, for use of his image analysis software and contributions to the early design and motivation of the experiment, and Isaac Hastings-Hauss, and undergraduate who helped with construction of the system.

Background

Classical kinetic theory requires molecular chaos and homogeneity [14, 17]. Atomic-scale collisions provide the source of homogeneous random motion in thermal systems and form the foundation of classical thermodynamics. In equilibrium thermal systems the crossover from ballistic motion to diffusive motion is a fundamental link between microscopic statistical mechanics and macroscopic thermodynamics [18]. In Einstein's classic thought experiment of a pollen grain in water a thorough study of the grain's ballistic motion would require simultaneous temporal resolution of $\simeq 10\mu\text{s}$ and spatial resolution of $\simeq 1\text{ nm}$ [19]. Therefore, this crossover from ballistic to diffusive has only recently been experimentally demonstrated in the equilibrium thermal systems of rarefied gases [20, 21] and liquids [22, 23].

By contrast, macroscopic systems allow studies of their constituent dynamics that are impossible in the thermal world. Macroscopic systems dilate the characteristic length and time scales but lose the stochastic excitations of thermal systems. This means that any of the random motion necessary for mimicking equilibrium thermal behavior macroscopically must be produced by some stochastic energy input. Because chaotic Faraday waves are very well understood and characterized they present an ideal source of randomness. The Faraday instability is excited on the surface of a fluid subject to vertical oscillations beyond some critical amplitude [12, 13, 24]. Above a second, higher, critical amplitude the surface waves transition from stable, ordered waves to spatio-temporal chaos [25]. Surface flows have been measured using fluorescent dyes [26, 27] and tracer particles considerably smaller than the characteristic wave size [26, 28–30]. A ballistic to diffusive crossover has been observed in chaotic Faraday waves using “virtual tracer” data drawn from particle image velocimetry measurements[31]. However, for real tracer measurements to date, diffusive motion and fractional Brownian motion have been observed at long and at relatively short time-scales, respectively [30, 32]; the full crossover from the ballistic regime to the diffusive regime for real particles has not been demonstrated before our present work.

It remains unproven, therefore, whether a driven (and therefore non-equilibrium), athermal system like chaotic Faraday waves still exhibit all characteristics of equilibrium statistical mechanics, such as a ballistic-diffusive crossover and a well-defined temperature derived from atomistic chaos, as it is in classical kinetic theory. A variety of attempts to define temperatures have been proposed for non-equilibrium systems [33]. These have had limited success, describing aspects of the systems’ dynamics only over narrow parameter ranges and for few measured properties. A typical approach is to use the Einstein relation [34, 35] or fluctuation-dissipation theorem [35] to define an effective temperature. While successful in producing a well-defined temperature, these studies do not comment on whether or not their internally determined quantities exhibit behavior consistent with classical kinetic theory. In the present study we achieve random excitation and homogeneity by floating a particle large relative to the characteristic length of the Faraday waves on a chaotic fluid surface (Figure 1). Despite the decidedly non-equilibrium nature of chaotic Faraday waves, we show that they drive a buoyant tracer to undergo fully ballistic (short times) and diffusive (long times) Brownian motion, a hallmark of isotropic equilibrium statistical mechanics. This system admits of a well defined temperature, diffusion

constant, and drag coefficient consistent with the system being a nearly ideal gas of excitations. We have created a macroscopic thermal-like system (which, if treated like a conventional thermal system would be one billion times hotter than the sun’s corona).

Methods

We generate the Faraday waves in a circular aluminum dish brim-full with water (Figure 1). We use a circular dish to discourage ordering of the waves [36]. The inner portion, where the water is held, has a radius of 9cm and a depth of 1.27cm. A gutter to collect spillover is carved around this inner region. The dish is vertically agitated by a shaker (Vibration Test Systems VTS-100) whose frequency f and peak-peak amplitude A we control independently using a digital function generator (Stanford Research Systems Model DS335) and a voltage amplifier (Behringer Europower EP4000). Mounted on the bottom of the dish is an accelerometer (CTC AC244-2D/010) used to measure stroke amplitude and frequency. The dish is filled to brim-full conditions [24] against a knife-edge to avoid pinning of the contact angle which would create a “cold” zone near the edges. However, the fluid position remains pinned to the knife edge leading to some damping of the waves near the edges. Our floating test particle is a 3D printed section of cone (selectively laser sintered nylon, coated in black spray paint, density approximately $.7\text{g/cm}^3$) with top radius $.75$ cm, height $.25$ cm, side angle 45 degrees, and mass 216 mg. The size of the particle is chosen such that it is always larger than the characteristic size of the Faraday waves which are on the order of millimeters. The particle is colored black and the dish is spray painted white for maximum contrast. The system is imaged from $\simeq 1.3\text{m}$ above the surface of the water with a digital camera (Pointgrey Flea3 FL3-U3-32S2M-CS with a Pentax C32500 KP lens) with a 2080x1552 CMOS sensor.

We know *a priori* that certain regions of our parameter space are inaccessible (Figure 2): below a critical amplitude line chaotic Faraday waves do not exist; above a sufficiently high amplitude line the surface undergoes a topological transition and begins to splash, which typically sinks the particle. The shape of these critical lines is non-trivially dependent on the properties of the fluid (i.e. viscosity, capillary length, skin depth), the frequency and amplitude of oscillation and the container aspect ratio [37]. The details of the transition from ordered to chaotic Faraday waves have been the subject of a great deal of scientific interest [38, 39]. However for this work we

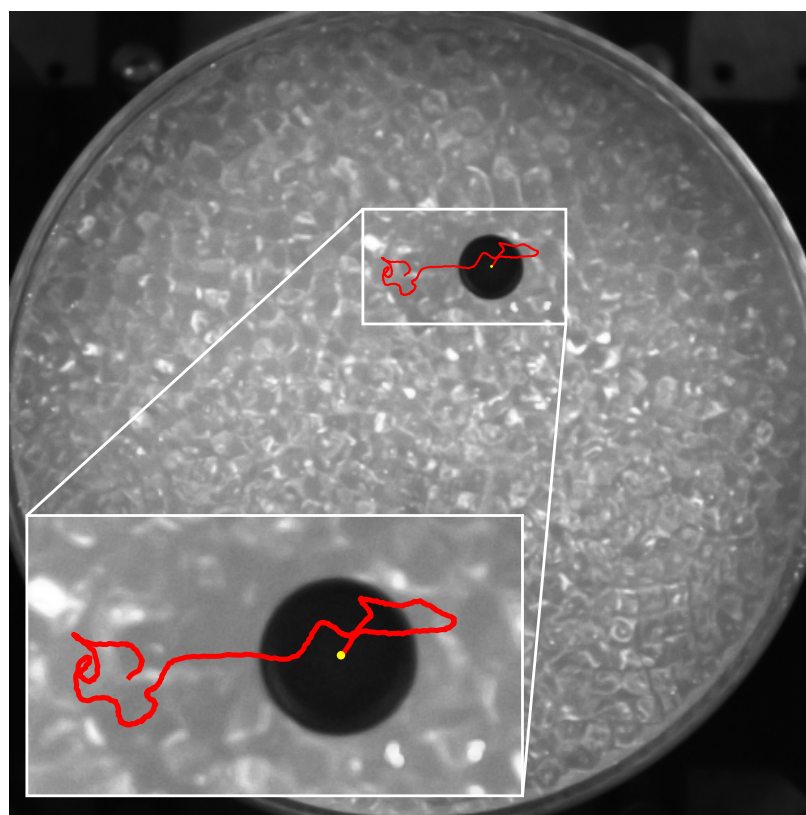
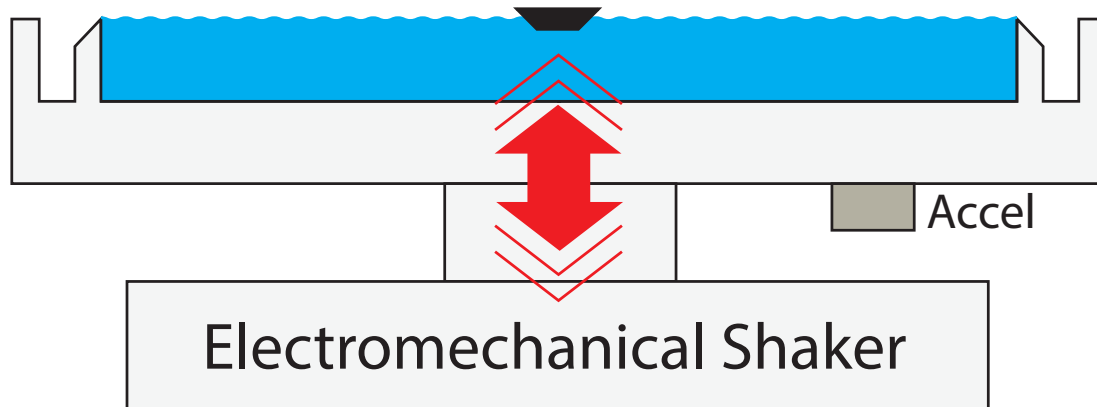


FIGURE 1. Experimental Apparatus

(cartoon) Cross-sectional diagram of shaker assembly. The inner portion of the dish is filled with water to brim-full conditions. The electromechanical shaker vertically agitates the dish, exciting the Faraday instability on the surface of the water. A buoyant particle is buffeted by the surface waves. An accelerometer is attached to the bottom of the dish to directly measure peak-peak amplitude A . (photo) Photo of the experimental apparatus from above. A floating particle is shown, along with a typical position trace for 7.5 seconds of data collection. The surface of the water is illuminated from an angle to show the chaotic Faraday waves.

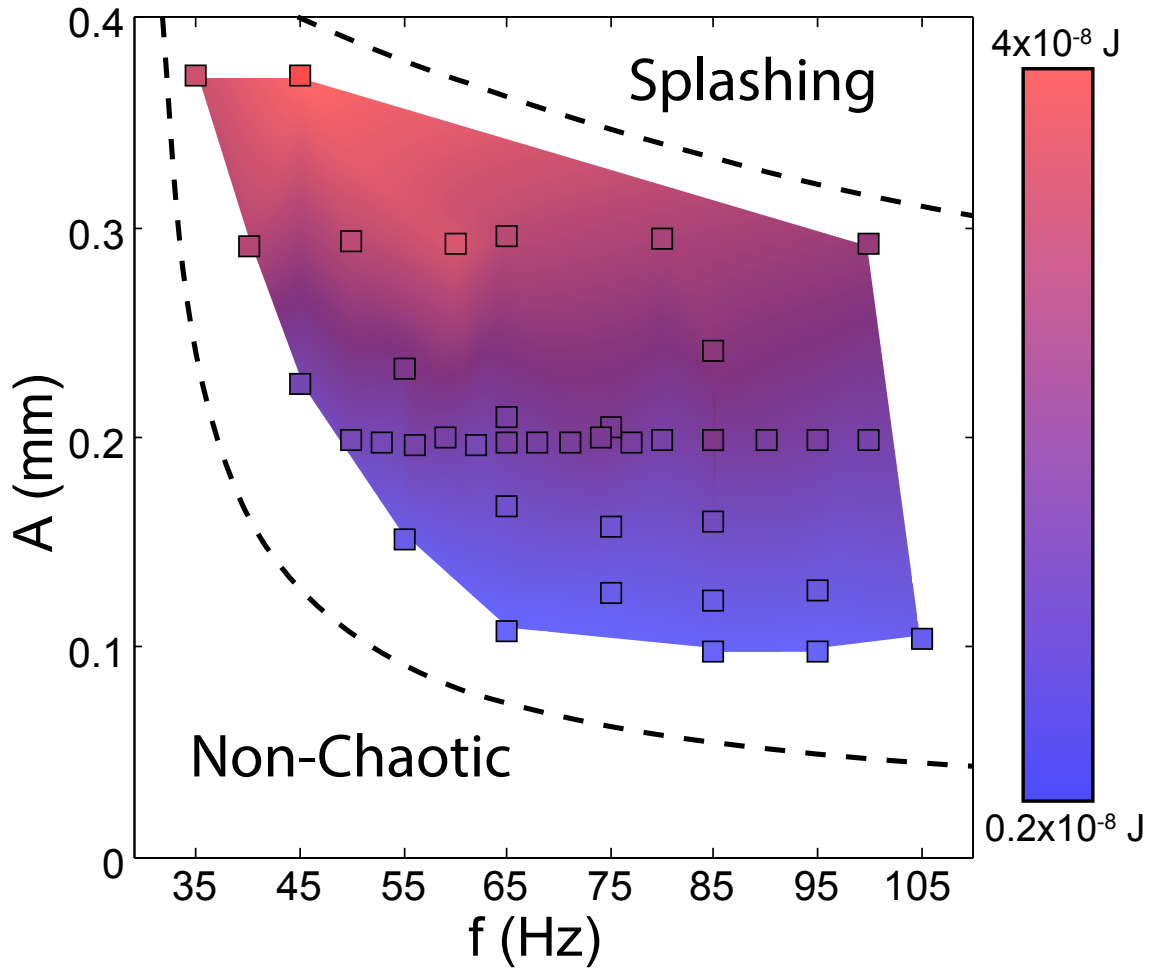


FIGURE 2. Map of parameter space.

The parameter space is formed by the two externally-controlled parameters, shaker frequency f and peak-peak amplitude A . This map shows approximate loci between the non-chaotic, accessible, and splashing regimes. Plotted within the accessible region are points in parameter space where measurements were taken, color indicating temperature T . Color gradient goes from blue (dark grey) for “cold” to red (light grey) for “hot.” Plotted behind these points is an interpolated contour map of T .

are only concerning ourselves with systems in which spatio-temporal chaos is fully developed, but the vertical oscillation is not so great that the fluid splashes.

The floating test particle is set into the dish near the center and tracking is initiated. We track the particle with sub-pixel accuracy using a radial symmetry algorithm [40]. By restricting our region of interest of the current frame to the area near where the particle was found in the previous frame, we are able to track in real time at 60 frames per second with a signal to noise ratio 200:1 and a sub-pixel real space resolution of $< 10\mu\text{m}$. The particle is tracked for 7.5 seconds, chosen to allow for maximum data collection while reducing the likelihood that the particle will reach the edge of the dish, where the physics is fundamentally different. The process is repeated for $N = 10$ or 100 trials.

We measure the mean square displacement $\langle \Delta r^2 \rangle$ and use it to characterize the particle's motion. If motion is ballistic then

$$\langle \Delta r^2 \rangle = \langle v^2 \rangle \Delta t^2, \quad (2.1)$$

where $\langle v^2 \rangle$ is the mean square ballistic velocity and Δt is the lag time. If motion is diffusive, then

$$\langle \Delta r^2 \rangle = 4D\Delta t, \quad (2.2)$$

where D is the diffusion constant. Figure 3 shows a representative mean square displacement demonstrating ballistic motion ($\langle \Delta r^2 \rangle \sim \Delta t^2$) for short times and diffusive ($\langle \Delta r^2 \rangle \sim \Delta t$) for long times. We measure the coefficients $\langle v^2 \rangle$ and D by fitting equations 2.1 and 2.2 to the data in the ballistic and diffusive regimes, respectively.

Results and Discussion

The insets of Figure 3a show the scaled distributions of displacement magnitude for various lag times Δt . For short times in the ballistic regime the distributions collapse when scaled by a factor of Δt , and for long times in the diffusive regime the distributions collapse when scaled by a factor of $\Delta t^{1/2}$. In both regimes, the distributions are well described by a two-dimensional Gaussian integrated over all directions uniformly. This random walk behavior is an emergent result of allowing a particle to interact with a chaotic surface.

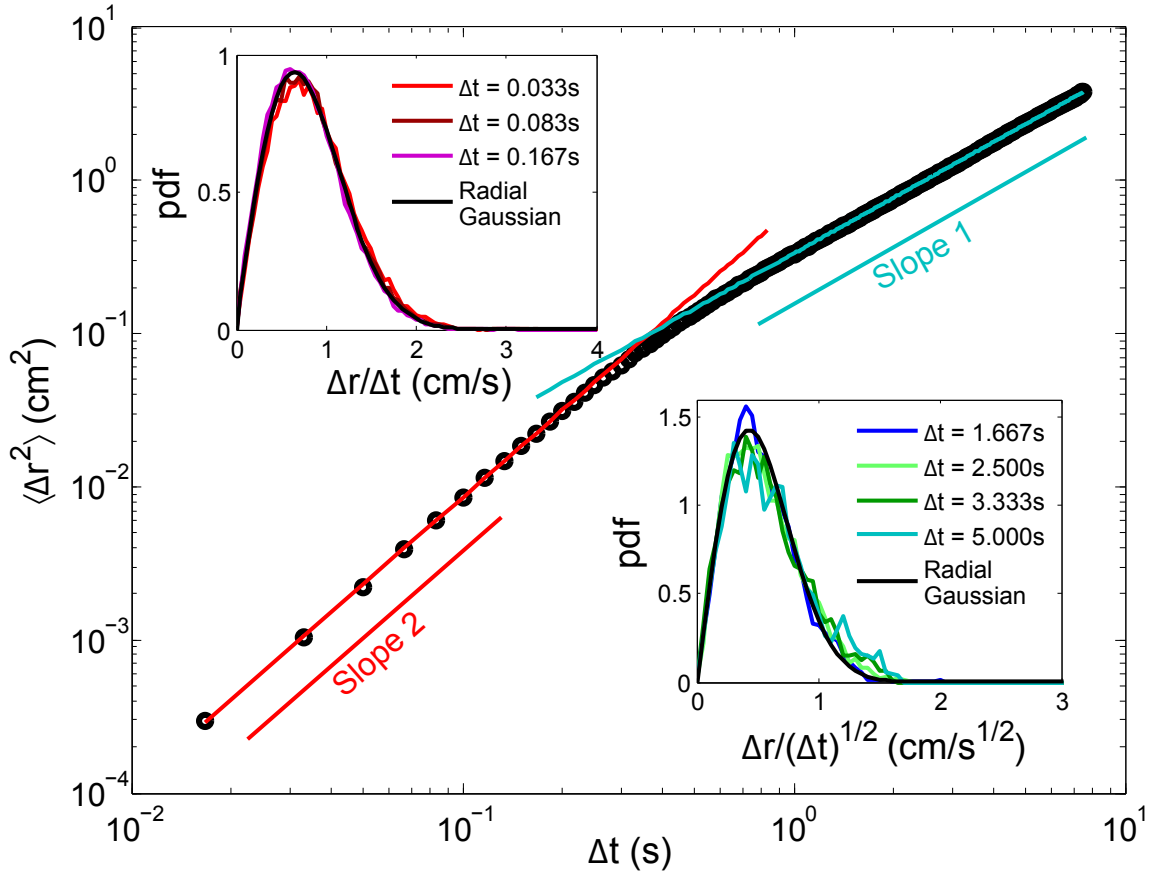


FIGURE 3. Ballistic and Diffusive Behavior

Representative mean squared displacement $\langle \Delta r^2 \rangle$ ($f = 85\text{Hz}$, $A = 0.159\text{mm}$). $\langle \Delta r^2 \rangle$ is plotted against lag time Δt . At short lag times the mean squared displacement shows a power law with an exponent of 2, indicating ballistic motion. For longer lag times the curve turns over to a power law with an exponent of 1, indicating diffusive motion. Inset in the upper left is the distribution of displacement Δr divided by a factor of lag time Δt for lag times in the ballistic regime. Inset in the lower right is the distribution of Δr divided by $\Delta t^{1/2}$ for lag times in the diffusive regime. Both distributions are shown to collapse onto a 2D Gaussian integrated over all directions (radial Gaussian).

In thermal systems the quantities $\langle v^2 \rangle$ and D are related to temperature T and the coefficient of viscous friction ζ . In contrast to studies such as [34, 35], we use the average kinetic energy of the tracer as it undergoes ballistic motion to define an effective temperature. By equipartition the temperature is proportional to the average kinetic energy per particle as

$$\frac{1}{2}m\langle v^2 \rangle = T, \quad (2.3)$$

where m is the mass of a particle ($m = 216\text{mg}$) and k_B the Boltzmann coefficient. We regard T as an energy, equivalent to $k_B T$ in molecular systems. T , D and ζ are related by the Einstein relation as

$$D\zeta = T \quad (2.4)$$

where D and ζ both depend on T . T may be treated with the same physics as a conventional temperature, as opposed to an “effective temperature” such as those used to describe granular and other athermal systems. The friction term ζ is primarily associated with the viscosity of the chaotic Faraday waves as a 2D medium through which the floating particle is moving. Thus, by measuring $\langle v^2 \rangle$ and D we can determine the intrinsic properties T and ζ of a 2D thermal-like system.

Analysis of the data reveals the dependence of $\langle v^2 \rangle$ and D , and therefore T and ζ , on our externally-controlled parameters A and f . Figure 4a demonstrates that temperature T is proportional to shaker amplitude A , independent of frequency. This trend is also apparent in the temperature contours shown in figure 2. Thus, driving amplitude is the external control for temperature. Since the typical Faraday wavelength is primarily determined by the driving frequency and T is independent of frequency, we may also deduce that T is independent of the ratio of particle size to wavelength over the range of parameters for which we have conducted our study. We find a calibration curve between driving amplitude and the temperature of our bath:

$$T \approx (1.3 \times 10^{-7} \frac{\text{J}}{\text{mm}})A - 1.0 \times 10^{-8} \text{J}. \quad (2.5)$$

The linearity of this relationship is expected because the height of the chaotic Faraday waves should be proportional to the driving amplitude, and the particle moves in response to the height difference between the two largest waves in contact with it. However, there is a curious feature to

this fit in that T crosses zero at finite A . This is due to the fact that below a particular driving amplitude the temperature is ill-defined because the Faraday waves are not chaotic. Thus, A must reach a critical value before T can exist and begin to increase.

While the existence of ballistic and diffusive motion is strongly suggestive that the system of driven Faraday waves can be considered as a gas at some temperature T , we can more rigorously examine whether other general properties of thermal gasses, such as the temperature dependance of their viscosity, manifest themselves in this driven system. Recalling now the Einstein relation (Eq. 2.4) we examine the behavior of the viscous drag coefficient ζ . Stokes' equation for incompressible fluids states that $\zeta \propto \eta$ where η is the viscosity. Sutherland's formula for the viscosity of a nearly ideal 2D gas (in which particles have finite collision radii and soft, long range interaction potentials) [41] further relates η to T as

$$\eta = \lambda' \frac{T}{\sqrt{T + C'}} \quad (2.6)$$

where λ' and C' are constants of the gas. We can now solve for D as a function of T for an ideal gas to find

$$D = a\sqrt{T + b}, \quad (2.7)$$

where all of our constants have been absorbed into a and b . Figure 4b shows our data on T and D to be well fit by this simple ideal gas model with constants $a = .16 \pm .01 \text{ m/kg}^{1/2}$ and $b = (-1.87 \pm 0.65) \times 10^{-9} \text{ J}$. The parameter a relates diffusion to energy and the parameter b contains information on the interactions within the gas.

As a relates diffusion to energy it has units of length/mass^{1/2}. Plugging in the length and mass scale of the particle we would predict from simple dimensional analysis that a should be on the order of $0.75 \text{ cm}/(0.2 \text{ g})^{1/2} \simeq 0.5 \text{ m/kg}^{1/2}$, which is comparable to the fitted value of a .

Since b is negative there is a positive value of T at which the diffusion constant should go to zero and thus the viscosity to infinity. This is a singular point that does not exist for real ideal gases but is difficult to probe directly because the timescales for diffusion diverge as $T \rightarrow -b$ and, more practically, it is near the transition from chaos to order in our system.

Above $T = -b$ the viscosity and diffusion constant maintain functional behavior consistent with that of a nearly ideal gas, suggesting that the chaotic Faraday waves should be considered a

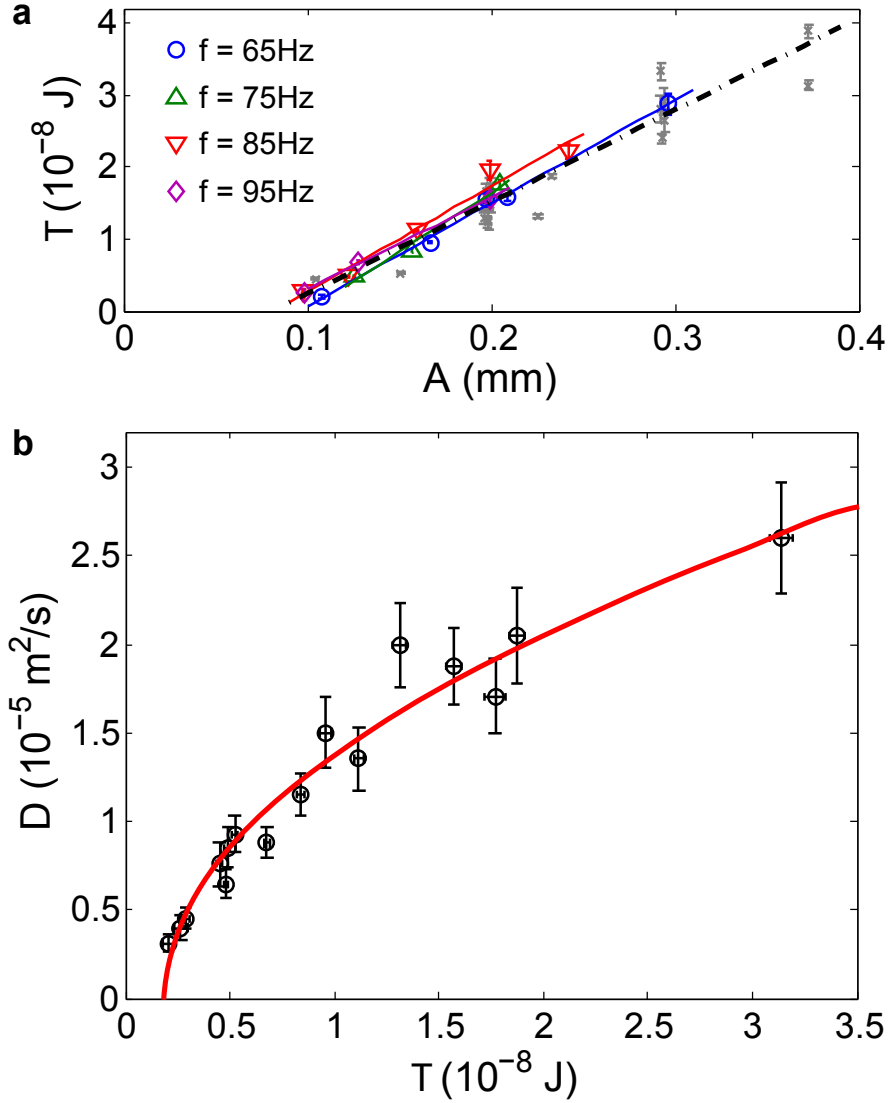


FIGURE 4. Gas behavior

- (a) temperature T plotted against shaker peak-peak amplitude A for various shaker frequencies f , with linear fits shown for frequencies plotted in large color symbols (circles, upward triangles, downward triangles, diamonds). Grey crosses are the remaining frequencies shown in figure 2, ranging from 35Hz-105Hz, and the dashed line is a linear fit to all data points shown. (b) Diffusion constant D plotted against temperature T . Data points are taken for data sets where $N = 100$ trials. Shown in red is a fit to the data of Equation 2.7. Error bars shown in (a) and (b) are 1σ confidence intervals resulting from fits used to determine D and T .

nearly ideal gas of random surface excitations. The sign of the constant b tells us the sign of the interaction between the elements of the gas: positive for attractive, and negative for repulsive. One would expect that the interactions in our system are repulsive, as gravity will cause waves to repel one another over short distances.

Conclusion

We have demonstrated for the first time that chaotic Faraday waves can be described as a thermal-like, nearly ideal gas of random surface excitations for which a thermal energy scale, diffusion constant, and viscosity are well defined. We directly observe the particle to receive normally distributed, isotropic kicks from the chaotic waves. The particle's displacement scales with lag time exactly as would be expected for a Brownian particle, and exhibits a clear transition from ballistic to diffusive behavior, showing that we have produced a laboratory-scale Brownian system by Aristotelian means. This thermal-like gas takes difficult-to-access time and length scales and dilates them to easily studied levels. In so doing we have defined a *macroscopic* effective temperature in an out-of-equilibrium system functionally identical to, but completely divorced in origin from a *microscopic* thermal temperature. The present single-particle study outlines the method by which one would define a temperature for a system of chaotic Faraday waves, and future studies will examine the dynamics of the multi-particle case.

This experimentally tractable system will be useful for studying the statistical mechanics of actively driven non-equilibrium systems in general, especially interparticle interactions and driven assembly on 2D substrates, which is a subject of active scientific interest [42]. An outstanding theoretical question for 2D systems is whether it is possible to create long range order from short-range interactions [43–45]. Our system offers a fully 2D environment in which these questions can be studied.

CHAPTER III

FLUIDS BY DESIGN: CHAOTIC SURFACE WAVES FORM A METAFUID THAT IS NEWTONIAN, THERMAL AND ENTIRELY TUNABLE

Abstract

In conventional fluids, viscosity depends on temperature according to a strict relationship. To change this relationship one must change the molecular nature of the fluid. Here, we create a metafluid whose properties are derived not from the properties of molecules, but rather from chaotic waves excited on the surface of vertically-agitated water. By making direct rheological measurements of the flow properties of our metafluid, we show that it has *independently* tunable viscosity and temperature, a quality that no conventional fluid possesses. We go on to show that the metafluid obeys the Einstein relation, which relates many-body response (viscosity) to single-particle dynamics (diffusion) and is a fundamental result in equilibrium thermal systems. Thus, our metafluid is wholly consistent with equilibrium thermal physics, despite being markedly non-equilibrium. Taken together, our results demonstrate a new type of material that retains equilibrium physics while simultaneously allowing for direct programmatic control over material properties.

As of this writing, this work has been accepted to but not yet published at *Proceedings of the National Academy of Sciences*. The writing and analysis were performed by me as primary author. Eric Corwin is listed as a coauthor as he advised this work. The material in this chapter is also coauthored with Alex Liebman-Peláez, an undergraduate who helped with construction of parts of the experimental system.

Background

Materials science seeks not only to understand, but to control the properties of matter. To do so, one must dynamically change the nature of conventional materials at the molecular scale. Recent work circumvents this problem by rejecting the molecule as the fundamental unit and substituting a macroscopic structural element. This approach has successfully created metamaterials with novel optical [1–3], acoustic [4–6], mechanical, [7–9] and fluid properties [10, 11] that would otherwise be impossible. However, this comes at a cost: by deriving their

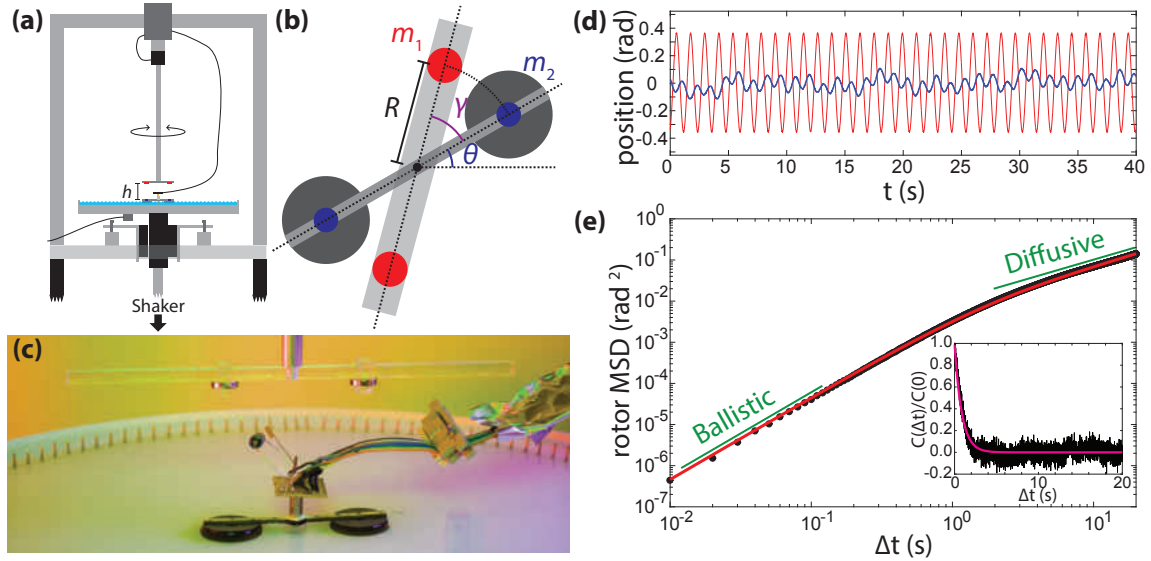


FIGURE 5. Experimental setup and Characterization

(a) The rheometer assembly. h is the vertical separation of the drive arm and test rotor. (b) Top-down cartoon illustrating the coordinates of the system. m_1 and m_2 are the moments of the drive arm and test rotor magnets, respectively, R is the radius of rotation of the magnets, θ is the angular position of the test rotor and γ is the relative angle between the drive arm and test rotor. (c) Photo of rheometer. (d) Example (Shaker: $f_s = 60$ Hz, $A_s = 0.064$ mm, drive arm: $\omega/2\pi = 0.8$ Hz) time series of drive arm (red, light) and rotor (blue, dark) positions. (e) Example (Shaker: $f_s = 60$ Hz, $A_s = 0.064$ mm) mean squared displacement (MSD). Our data (points) shown with the prediction for a truly Brownian particle (line) [46, 47]. (inset) Velocity autocorrelation function corresponding to the plotted MSD, with the prediction of the Langevin equation plotted over the data.

properties from macroscopic, non-equilibrium, or anisotropic elements, these materials necessarily abandon the physics of thermal systems. In this work, using a combination of active and passive rheology we show that macroscopic chaotic surface waves on a vertically agitated fluid form a fully thermal metafluid with dynamically tunable material properties. In contrast to a conventional fluid in which viscosity and temperature are inextricably linked, we show that these quantities are *independently* tunable in our system. We further demonstrate that by satisfying the barest criteria of isotropy and steady-state chaos (as required by kinetic theory [14, 17]) we have created a system that obeys the Einstein relation [19]. Thus, despite being macroscopic and non-equilibrium, it is well-described by equilibrium thermal physics.

The “molecules” of our metafluid are chaotic Faraday waves [12, 13], generated in a water-filled aluminum dish that is vertically oscillated with RMS amplitude A_s and at frequency f_s (Figs. 5(a) & (c), see chapter 5 for technical details). The waves uniformly cover the surface of the

water and only experience significant pinning at the boundary, far from where our measurements are conducted. The chaos and wave density is holistically steady state, though the existence of a particular wave is transient. Thus, “collisions” in our system refer to encounters between a buoyant tracer and the ephemeral excitations of the chaotic wave environment. We have previously shown chaotic Faraday waves to have a well defined temperature decoupled from the bath temperature by observing the Brownian motion of a tracer particle [15]. We found this temperature to be proportional to shaker amplitude.

Results and Discussion

Drag coefficient

Our rheometer consists of a driving arm that applies a sinusoidally varying torque $\tau(t)$ at a variable frequency to a buoyant test rotor via a magnetic interaction (Figs. 5(a), (b) & (c), see chapter 5 for technical details). We derive the exact form of this torque in chapter 5 and find that it is well approximated as a Hookean interaction between the drive arm and the test rotor with rotational spring constant $k_r \approx 6 \times 10^{-5}$ Nm (Fig. 14 in chapter 5). Sample time series for the drive arm and test rotor positions are given in Fig. 5(d).

We program the driving arm’s position β to oscillate sinusoidally as

$$\beta(t) = \beta_0 \sin(\omega t), \quad (3.1)$$

where β_0 is the oscillation amplitude and ω is the angular driving frequency. The resulting motion of the test particle is described by the differential equation

$$I\ddot{\theta} = \tau(t) - \zeta_r \dot{\theta}, \quad (3.2)$$

where θ is the angular position of the test particle and I is the moment of inertia. Treating the rotor as a damped driven harmonic oscillator, the solution to this differential equation is

$$\theta(t) = \theta_0 \sin(\omega t + \phi), \quad (3.3)$$

where the response frequency ω is identical to the driving frequency ω after a brief period as the rotor relaxes into its steady oscillation. All data sets are collected after allowing for this transient period. As derived in chapter 5, the driving amplitude β_0 , oscillation frequency ω , response amplitude θ_0 and phase lag ϕ are related to the drag coefficient ζ_r as

$$\zeta_r = \frac{k_r \beta_0}{\omega \theta_0} \sin \phi. \quad (3.4)$$

The rotor's response $\theta(t)$ is recorded using a contactless magnetic encoder, then the response amplitude and phase lag are obtained by using a simple lock-in measurement.

In Fig. 6(a) we demonstrate that the metafluid behaves as a Newtonian fluid with a drag coefficient that is independent of the rheometer drive frequency over an experimentally relevant range of ω . The above equations also predict (as shown in chapter 5) a mechanical impedance of

$$Z_m(\omega) = \sqrt{\left(\frac{\zeta_r}{I}\right)^2 + \frac{1}{\omega^2} \left(\frac{k_r}{I} - \omega^2\right)^2}. \quad (3.5)$$

Figure 6(b) demonstrates that the measured impedance agrees with the expected form.

Fig. 6(c) shows the results of our active measurement of drag coefficient at values for shaker amplitude and frequency covering the phase space of chaotic Faraday waves. We find that the viscous drag coefficient imparted by the chaotic waves is proportional to the product $A_s f_s$. We can make a heuristic argument to show that this relationship is reasonable. If we hold the shaker amplitude A_s fixed and increase the shaker frequency f_s we will decrease the characteristic wavelength of the surface waves and thus decrease the characteristic time between collisions of the waves and the rotor. If we look to the derivation of the Einstein relation we see that ζ_r should be inversely proportional to this characteristic time [19] and thus find $\zeta_r \propto f_s$. Likewise, if we hold f_s constant and increase A_s we will increase the energy in each surface wave, thus increasing the momentum transfer effected by each collision and so increasing the drag coefficient.

The onset of chaos limits our measurement range in shaker amplitude and frequency space, because there exist regions in this space for which the Faraday waves are not chaotic (or indeed, do not even exist). Nonetheless, we measure the drag coefficient on calm water to be $\zeta_r = 1.9 \times 10^{-5}$ Js, slightly below the lowest drag coefficient that we are able to measure with chaotic waves.

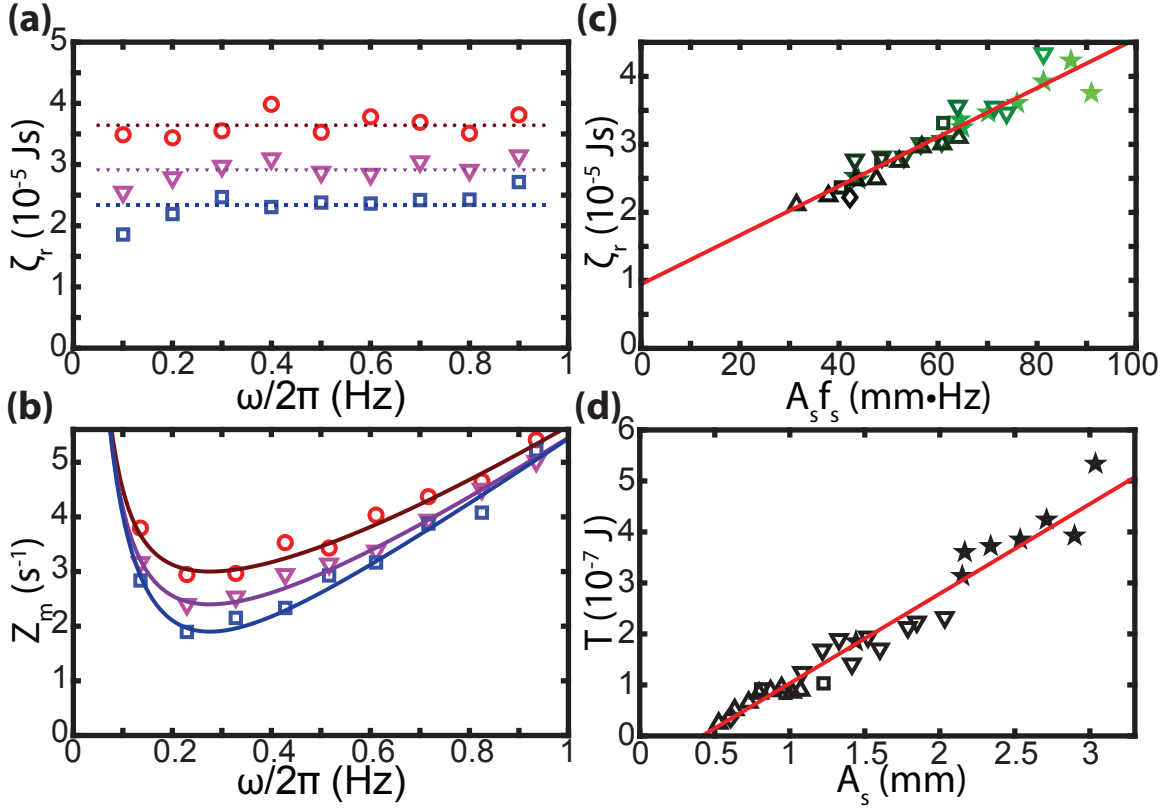


FIGURE 6. Tunable Newtonian Fluid Behavior

(a) Demonstration that measured drag coefficient ζ_r is independent of drive arm frequency ω at $A_s = 0.85$ mm and $f_s = 50$ Hz (squares), $A_s = 1.2$ mm and $f_s = 50$ Hz (triangles), and $A_s = 2.4$ mm and $f_s = 30$ Hz (circles). Dotted lines are mean drag coefficient at each amplitude.

(b) Mechanical impedance Z_m measured at different drive arm frequency ω . Marker shape indicates the same values of A_s and f_s as in (a). Solid lines are the expected $Z_m(\omega)$ for a damped driven harmonic oscillator. (c) Fitted calibration curve relating rotational drag coefficient to the

product of shaker amplitude A_s and shaker frequency f_s . Best fit shown is $\zeta_r \approx (3.6 \times 10^{-7} \text{ Js}/(\text{mm Hz}))A_s f_s + 9.4 \times 10^{-6} \text{ Js}$. Marker color illustrates amplitude; dark to light gradient corresponds to low to high amplitude variation. Marker shape indicates shaker frequency: $f_s = 30$ Hz (stars), $f_s = 40$ Hz (inverted triangles), $f_s = 50$ Hz (squares), $f_s = 60$ Hz (upright triangles), and $f_s = 70$ Hz (diamonds). (d) Fitted calibration curve relating wave

temperature T to shaker amplitude A_s . Best fit shown is $T \approx (1.8 \times 10^{-7} \text{ J/mm})A_s - 7.3 \times 10^{-8} \text{ J}$. Marker shape indicates shaker frequency, as in (c).

Temperature and diffusion constant

To make passive measurements, we remove the driving arm of our rheometer and thus allow the test rotor to diffuse freely while tracking its position. From the position trace we calculate the mean squared displacement (MSD) $\langle(\Delta\theta)^2\rangle$ and extract two quantities: a mean squared ballistic angular velocity $\langle\omega_b^2\rangle$ and a rotational diffusion constant D_r . A sample MSD is shown in Fig. 5(e). Plotted over our data in Fig. 5(e) is the prediction by Ornstein and Fürth for the MSD of a truly Brownian particle [46, 47]. Set into Fig. 5(e) is the velocity autocorrelation corresponding to the plotted MSD, shown with the prediction of the Langevin equation for a thermally diffusing particle. The agreement of predicted thermal behavior with our data demonstrates that our system has the same constituent dynamics as a thermal particle, albeit at much larger length and time scales.

For sufficiently small lag times Δt , the MSD appears ballistic: $\langle(\Delta\theta)^2\rangle_{\Delta t_b} = \langle\omega_b^2\rangle\Delta t_b^2$. At longer times, the MSD appears diffusive: $\langle(\Delta\theta)^2\rangle_{\Delta t_d} = 2D_r\Delta t_d$. To avoid the biases associated with the traditional method of fitting the MSD to estimate $\langle\omega_b^2\rangle$ and D_r , we instead choose the smallest lag times Δt_b and Δt_d that are convincingly ballistic and diffusive [48], respectively, and estimate $\langle\omega_b^2\rangle$ and D_r using

$$\langle\omega_b^2\rangle = \frac{\langle(\Delta\theta)^2\rangle_{\Delta t_b} - \sigma^2}{\Delta t_b^2} \quad (3.6)$$

and

$$D_r = \frac{\langle(\Delta\theta)^2\rangle_{\Delta t_d} - 2\sigma^2}{2\Delta t_d} \quad (3.7)$$

where $\sigma^2 = 3.7 \times 10^{-5} \text{ rad}^2$ is the positional error associated with the discrete nature of the magnetic rotary encoder output. Finally, given the hydrodynamic moment of inertia I_h for the rotor, equipartition gives us the temperature as $T = I_h\langle\omega_b^2\rangle$.

Fig. 6(d) confirms our previous finding that temperature is proportional to shaker amplitude A_s [15]. We would expect the temperature of the system to be proportional to the energy density in the surface waves, which is itself proportional to the amplitude squared as $T \propto A_{waves}^2$. We can understand the linear dependence of T on the shaker amplitude A_s by considering the response properties of Faraday waves. In such systems, the characteristic response amplitude is generally proportional to the square root of the driving amplitude [49], so $A_{waves} \propto A_s^{1/2}$ which leads to $T \propto A_s$.

The temperatures we measure here from rotational motion are consistent with the temperature we measured in earlier work on translational motion [15], giving further credence to the notion that our system demonstrates energy equipartition and is truly thermal. The measured temperature is a remarkable 14 orders of magnitude larger than the water bath temperature, demonstrating that the thermal behavior of our system is completely divorced from that of ordinary matter.

Einstein relation and hydrodynamic moment of inertia

Thermal fluids satisfy the Einstein relation, which states that $D_r \zeta_r = T$. The power of the Einstein relation is that it connects two very different properties of fluids: rheology (a measurement of correlated many-body behavior) and diffusion (a measurement of single-particle dynamics). There is no *a priori* reason to expect the Einstein relation to hold in a non-equilibrium complex fluid such as ours in which energy is constantly being injected into the system. Nonetheless, Fig. 7(a) demonstrates that the Einstein relation is satisfied. That we discover an intact Einstein relation further convinces us that our macroscopic metafluid is in fact an equilibrium fluid. Additionally, Fig. 7(b) shows that the diffusion constant calculated from the MSD is consistent with the diffusion constant as calculated using the Green-Kubo relations, which relate the diffusion constant to the integral of the velocity autocorrelation function. This consistency convinces us that Einstein relation in our system may be trusted over all timescales available to our measurement. Taken together, these results suggest that the universality of thermal systems should be extended to systems which satisfy broader criteria of steady-state chaos and isotropy.

This notion of universality is supported by work done in other driven, dissipative systems. For example, the work of Ojha *et al.* [50] demonstrated that a particle agitated by turbulent airflow is identically thermal with a temperature completely divorced from the room temperature. Here, we have used a new mechanism for thermalization yet nevertheless recover thermal behavior, also with with a temperature completely divorced from that of the surroundings. Our work further demonstrates that these macroscopic thermal systems can be tuned in ways that microscopic systems cannot.

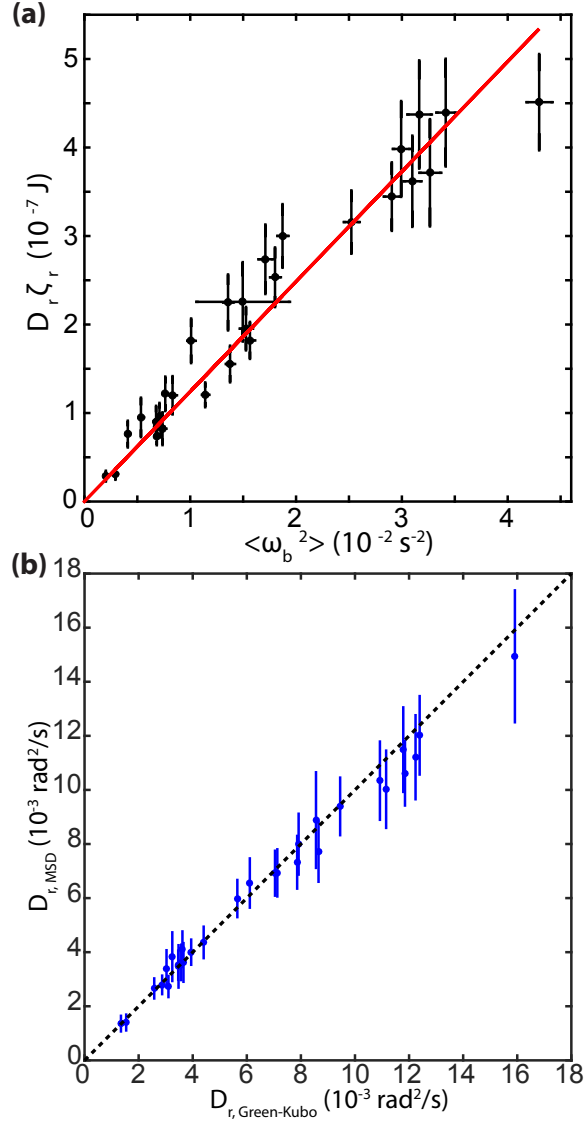


FIGURE 7. Einstein Relation and Green-Kubo Relation

- (a) Demonstration of the Einstein relation in our system. The product $D_r \zeta_r$ is proportional to the angular mean square ballistic velocity $\langle \omega_b^2 \rangle$, which is in turn proportional to the effective temperature of the waves T . The line shown is a fit to the data of the Einstein relation $D_r \zeta_r = I_h \langle \omega_b^2 \rangle$, with the hydrodynamic moment of inertia I_h left as a free parameter, determined by the fitting to be $I_h = 1.2 \times 10^{-5}$ kg m 2 . The error bars shown are 1σ confidence intervals determined from the calculation of D_r and $\langle \omega_b^2 \rangle$. (b) Comparison of diffusion constant measured from MSD ($D_{r,MSD}$) and using the Green-Kubo relations ($D_{r,Green-Kubo}$). The dashed line has slope 1, indicating good agreement between the two methods of calculating D_r .

The slope of the fitted line relating $\langle \omega_b^2 \rangle$ and $D_r \zeta_r$ in Fig. 7(a) is the hydrodynamic moment of inertia I_h , as $T = I_h \langle \omega_b^2 \rangle$. This quantity is larger than the moment calculated directly from the mass and geometry of the test rotor by nearly an order of magnitude due to the fact that a volume of water is swept along with the rotor.

We have thus far shown that $T \propto A_s$, $\zeta_r \propto A_s f_s$ and $D_r \zeta_r = T$. Taken together, these results imply that $D_r \propto 1/f_s$. We can heuristically understand this relationship by realizing that shaker frequency is inversely related to the characteristic wavelength of the chaotic surface waves. As shaker frequency decreases, the characteristic wavelength increases. Since the average distance between wave excitations is greater, the mean free path and mean free time of a diffusing particle increase proportionally. The diffusion constant is proportional to (mean free path)²/(mean free time). By this line of reasoning, D_r should be proportional to $1/f_s$.

Our results also imply that D_r should not depend strongly on shaker amplitude A_s . We can understand this heuristically as well. As the shaker amplitude increases, so too does the amplitude of the waves, as we outlined in our discussion of why $T \propto A_s$. This increases the strength of the kicks that set a particle in motion, but also increase the strength of the kicks that slow it down. The increase in thermal energy is offset by the energy dissipated by the drag coefficient, which also increases with shaker amplitude. Thus, it is reasonable that D_r not depend strongly on A_s .

Tunable thermal Newtonian metafluid

We have demonstrated three properties of this metafluid: 1) The metafluid has a well-defined Newtonian viscous drag which is controlled by the product of shaker amplitude and frequency. 2) The metafluid has a well-defined temperature which is controlled by shaker amplitude. 3) The metafluid satisfies the Einstein relation. These results lead to the inevitable conclusion that our system is in fact a thermal Newtonian metafluid with independently tunable material properties as shown in Fig. 8. Any arbitrary state or path in $D_r - \zeta_r - T$ space that satisfies the Einstein relation is translatable using our measured calibration curves into the $f_s - A_s$ parameter space. An example $D_r - \zeta_r - T$ path is shown in red in Fig. 8(a), then shown translated into a corresponding $f_s - A_s$ path in Fig. 8(b) using the Einstein relation and the calibration curves shown in Figs. 6(c) and (c).

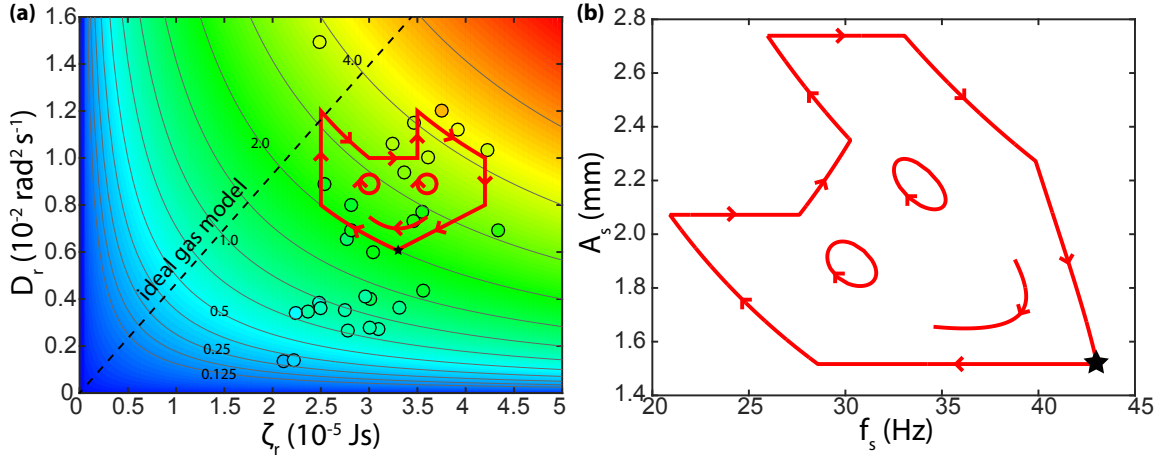


FIGURE 8. Phase Space and Parameter Space

(a) Phase space. Measured diffusion constant plotted against measured drag coefficient (circles). Marker color indicates measured temperature, which is in reasonable agreement with the background gradient that represents temperature as calculated from the Einstein relation, $T = D_r \zeta_r$. Example isotherms (black lines) are shown, labelled in units of 10^{-7} J. Our system can take any path along the surface defined by the Einstein relation, whereas a conventional fluid is confined to a particular curve (ideal gas behavior shown as an example). An example path through $D_r - \zeta_r - T$ phase space beginning at the star is plotted, and is then transformed into $f_s - A_s$ parameter space (b) via the Einstein relation and the calibration curves shown in Fig 6(c) and 2(d).

The surface defined by the Einstein relation is shown as the background gradient in Fig. 8(a), with color indicating temperature. Each trial measurement of our system is able to sit anywhere along this surface as shown by the plotted points in Fig. 8(a). The color of the plotted points indicates the measured temperature for that trial, and we see, as in Fig. 7(a) that our system agrees with the Einstein relation.

Conventional fluids, by contrast, lack the freedom to move arbitrarily about this surface, as they suffer from the additional constraint that viscous drag is a function of temperature. For example, viscous drag in an ideal gas is related to temperature as $\zeta \propto T^{1/2}$ (and thus $\zeta \propto D_r$) as shown in the representative ideal gas model curve in Fig. 8(a) (dashed line). To change the constant of proportionality one would need to change the molecular composition of the gas or, put more plainly, one would need to change the very identity of the gas. A conventional fluid is therefore confined to a single curve through $D_r - \zeta_r - T$ space.

Conclusion

In this paper we have presented a fully tunable, thermal Newtonian metafluid. By combining passive and active rheology we directly measure diffusion, temperature, and viscous drag in a system of chaotic surface waves and show that they are independently manipulable. The Einstein relation is satisfied even though our system is both macroscopic and non-equilibrium, hinting that a broader universality exists in random systems: so long as steady-state, isotropic chaos exists, the system may be mapped onto an equilibrium statistical mechanical system. This reading of the data is supported by previous studies of thermal behavior in driven, dissipative systems with inherent randomness [50].

We have followed in the footsteps of previous metamaterial research [1–11], creating and characterizing a novel material by rejecting the atom as the fundamental thermal unit and substituting a macroscopic element, in our case, chaotic surface waves. Our system provides a novel platform in which experiments may be performed, where the tools of thermodynamics remain intact and the fluid properties can be controlled in real time. There are obvious limitations, for example, the metafluid can't flow through a pipe, it can't be compressed nor is there an easy way to define pressure, and it is confined to two dimensions. However, we have already shown it to be useful in observing the atomistic dynamics of 2D polymer analogs [16], and we believe that it will prove elucidating in many open questions of the thermal world, such as self-assembly and 2D pattern formation [51–53]. Perhaps, emergent metafluids such as ours exist throughout the macroscopic world, be they swarms, turbulent weather, financial markets or any other system with intrinsic randomness.

CHAPTER IV

EXPERIMENTAL AND COMPUTATIONAL STUDY OF MACROSCOPIC ANALOGS TO SHORT CHAIN MOLECULES: AN ATOMISTIC APPROACH

Abstract

We use a bath of chaotic surface waves in water to mechanically and macroscopically mimic the thermal behavior of a short articulated chain with only nearest-neighbor interactions. The chaotic waves provide isotropic and random agitation to which a temperature can be ascribed, allowing the chain to passively explore its degrees of freedom in analogy to thermal motion. We track the chain in real time and infer end-to-end potentials using Boltzmann statistics. We extrapolate our results, by using Monte Carlo simulations of self-avoiding polymers, to lengths not accessible in our system. In the long chain limit we demonstrate universal scaling of the statistical parameters of all chains in agreement with well-known predictions for self-avoiding walks. However, we find that the behavior of chains below a characteristic length scale is fundamentally different. We find that short chains have much greater compressional stiffness than would be expected. However, chains rapidly soften as length increases to meet with expected scalings.

This work was originally published in *Physical Review E* [16]. The writing and analysis were performed by me as primary author. Eric Corwin is listed as a coauthor as he advised this work. The material in this chapter is also coauthored with Clayton Kilmer, an undergraduate who helped with data collection.

Background

Anyone who has ever put the wrong weight motor oil into a car engine can attest to the fact that the length of a chain molecule largely determines its mechanics [54]. A low-weight oil may be too thin and a high-weight oil too viscous for efficient operation. Biopolymers such as DNA also evidence changing mechanical behavior with changing length. Recent work shows that short strands are far more flexible than would be expected from simply scaling down the behavior of long strands [55]. Understanding this scale dependence in polymers is crucial to creating new materials, as is being done with polymer thin films [56, 57] and so-called “DNA origami” [58, 59]. Polymer mechanics is well explored in the coarse-grained sense, with many

established methods for direct measurement [60–62] and simulation [63–66]. However, there is scant experimental evidence directly relating whole polymer mechanical properties to behavior at the single bond level. These questions have been addressed in macroscopic granular polymer studies [67, 68] however such systems lack a thermodynamic temperature, muddying the link to true thermal systems. Statistical physics predicts [69], and empirical studies confirm [70] that the end-to-end potential of a sufficiently long polymer chain is harmonic, regardless of the microscopic interactions. Similarly, universalities are predicted for the scaling of statistical parameters (i.e., variance and mean) of both bond winding angle [71] and linear dimension [72, 73] in a polymer chain when considered as a self-avoiding walk (SAW). While this is a powerful and robust result regarding the chain-scale mechanics, it does little to elucidate the behavior towards the monomer scale, as it does not address short chains.

Materials and Methods

In this paper we build a macroscopic analog to polymer physics in a bottom-up fashion which allows us to observe not only chain-scale but also true monomer-scale behavior. We find that short polymer chains exhibit behavior fundamentally different than that predicted for their long counterparts. We use chaotic Faraday waves to create a macroscopic thermal-like bath with a well-defined temperature T , as we have previously described in reference [15]. The waves are generated by vertically oscillating a circular aluminum dish with a diameter of 17.5 inches and a depth of 0.5 inches (Fig 9a). The dish is mounted on a ceramic-coated aluminum shaft (diameter 2 inches), which passes through a 2 inch inner diameter air bushing (New Way Air Bearings). This assembly is leveled by a stage mounted to the outside of the bushing mounting block. The ceramic coated shaft is connected by a 24 inch length of 1 inch T-slot framing to an electromechanical shaker (Vibration Test Systems VTS-100) powered by a digital function generator (Stanford Research Systems Model DS335) through a voltage amplifier (Behringer Europower EP4000). An accelerometer (CTC AC244-2D/010) is mounted to the bottom of the dish to measure stroke amplitude and frequency.

We 3D-print our macroscopic polymer analogs in a clear photopolymer resin using a Formlabs Form1. Our macroscopic polymer consists of two basic elements: buoyant particles and links. The particles are cylindrical boats (diameter 15mm, height 3mm) with centered masts

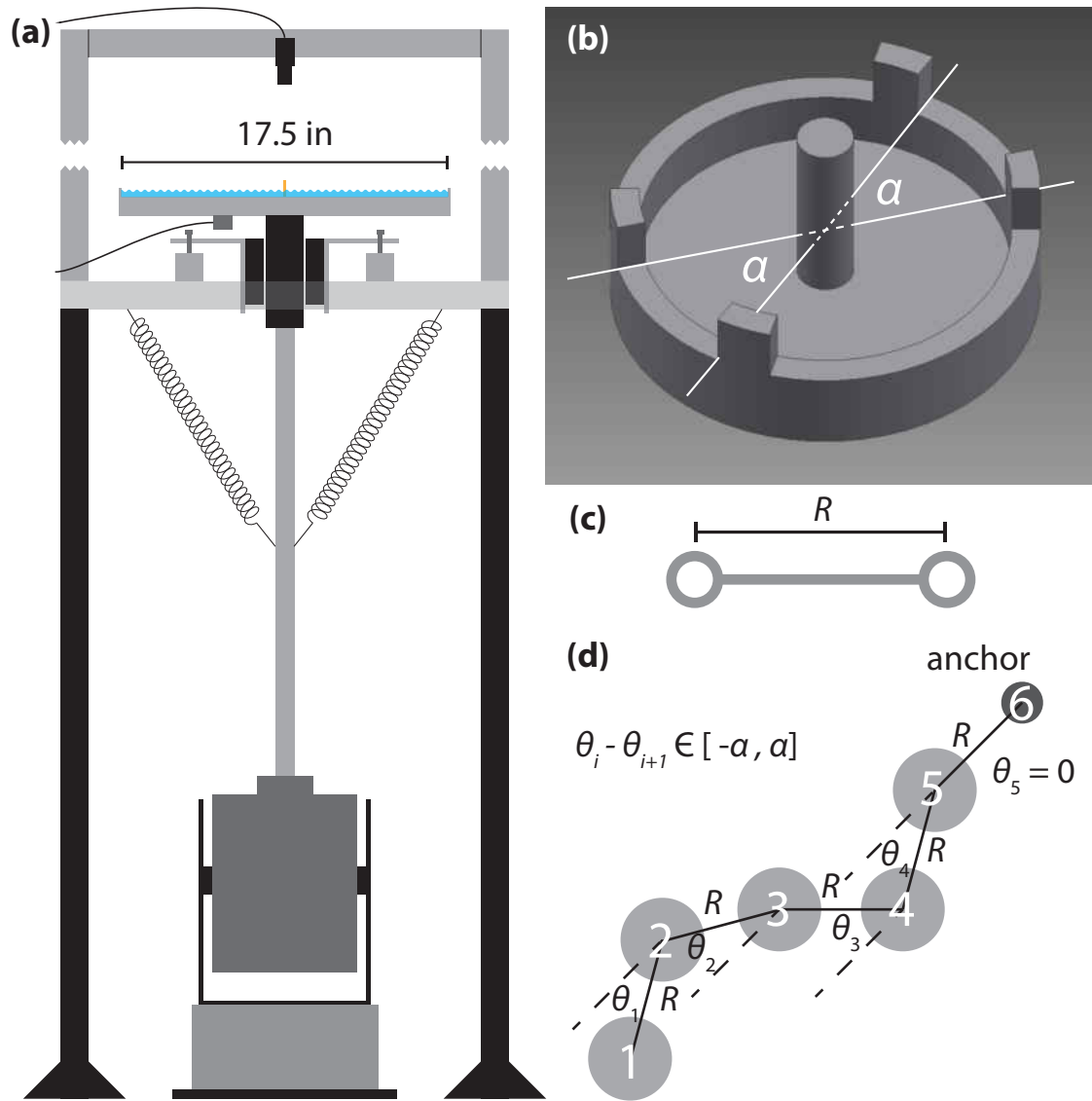


FIGURE 9. Experimental Design

(a) The shaker assembly. (b) 3D schematic of one for the buoyant particles in the chain, showing the definition of restricting angle α . (c) A link showing fixed length R . (d) A chain, demonstrating the measurement of link angle θ_i . Bulk rotations are eliminated from our coordinate system by measuring all θ_i off of the link most proximal to the anchor. This allows us to work exclusively in terms of the relative coordinates of members of the chain.

(diameter 2mm, height 7.5mm). The links are rods with loops at each end, separated by 22mm on center, that slide over the masts to link the boats together in a chain (Fig. 9c). Bond angle is restricted by stops on the gunwales of the boats (Fig. 9b) separated by an angular distance α . This chain is attached to a brass post set into the center of the aluminum dish using a link that is free to rotate about the anchor point. This prevents the chain from interacting with the boundary of the dish, where the physics is fundamentally different, and allows us to gather data for arbitrarily long amounts of time, in our case 8 hours. In this study we present data for: 1) a chain with $\alpha = \pi/4$ consisting of the post plus five other particles, five links, and 2) a chain with $\alpha = \pi/6$ consisting of the post plus eleven particles, and eleven links.

To facilitate automated tracking each boat has a circular well imprinted in the bottom with a diameter 1/2 that of the boat itself, uniformly filled with black oil paint. The anchor post is capped with a black tracking point. The positions of these black spots are tracked in real time at 30 frames per second (Pointgrey Flea3 USB camera with a Pentax C32500 KP lens, mounted 8 feet above the dish) using a radial symmetry algorithm [40]. To gather data on the dynamics of the chain we vertically oscillate our system with a frequency of 40Hz and an amplitude of 0.18mm peak-to-peak creating a temperature of about 1.3×10^8 J. These parameters were chosen such that the Faraday waves would be well into the chaotic regime without causing the water to splash and capsize the boats. We are limited in the length scales that we may probe in our system. Particles or chains smaller than the typical Faraday wavelength (on the order of millimeters) will not receive thermal-like agitation. Chains longer than the diameter of our dish (44.5 cm) can interact with the side walls. The dish size was chosen as to allow for the largest possible system while still remaining within the driving capability of our shaker.

Data Analysis and Simulation

In Figure 10 we demonstrate that the instantaneous bond angle velocities induced by the chaotic waves are uncorrelated in a chain of rigidly linked particles for times longer than the ballistic timescale (about 0.3 s). The motion of a given bond angle is initially anticorrelated with its immediate neighbor due to the buckling of a chain of rigid links. As a bond angle is kicked in one direction, its neighbor must react in the opposite direction as a result of the constraints in the system. More distant neighbors show weak correlations that die off quickly. The 10Hz oscillation

in correlation results from the beating between the dish oscillation frequency (40Hz) and the imaging frequency (30Hz). The lack of correlation beyond that induced by buckling of the chain allows us to rule out the possibility of non-thermal correlations between particles.

To simulate the behavior of chains longer than experimentally accessible we employ a simple unbiased Monte Carlo algorithm to simulate each chain as a SAW. We begin by generating a random walk with N bond angles where each step is of length R and taken in a direction drawn from the distribution of bond angles

$$p(\phi_{i,i+1}) \propto e^{-V_\phi(\phi_{i,i+1})/T} \quad (4.1)$$

created by a given potential V_ϕ . The random walk is then checked for overlaps of the boats and/or the links. If there are any overlaps, the chain is thrown out. If there are no overlaps then the chain is indeed a SAW and the end-to-end distance and winding angle are computed. This process is repeated until the data for 10^6 valid SAWs of length N have been collected.

We follow the Flory convention [73], which utilizes bond lengths and bond angles to describe a polymer in generalized nearest-neighbor coordinates (Fig. 9d). To coarsen beyond nearest-neighbor coordinates, we represent the configuration of the chain in terms of radial distance $r_{i,j}$ between particles i and j and a winding angle between bonds i and j defined as

$$\phi_{i,j} = \sum_{m=i}^{j-1} (\theta_m - \theta_{m+1}), \quad (4.2)$$

where θ_i is the angle of the i th bond with respect to the link nearest the anchor point. The use of a bond winding angle ensures that the angles we deal with are cumulative quantities and not bounded between $\pm\pi$. Note that, since $n_{bonds} = n_{particles} - 1$, the winding angle $\phi_{i,j}$ corresponds to the interparticle distance $r_{i,j+1}$.

We use Boltzmann statistics to measure effective potentials for the winding angle V_ϕ and the radial distance V_r . We relate the probability distributions of winding angle $p(\phi_{i,j})$ and end-to-end distance $p(r_{i,j})$ to the underlying potentials scaled by the temperature T [15] as

$$p(\phi_{i,j}) \propto e^{-V_\phi(\phi_{i,j})/T} \quad (4.3)$$

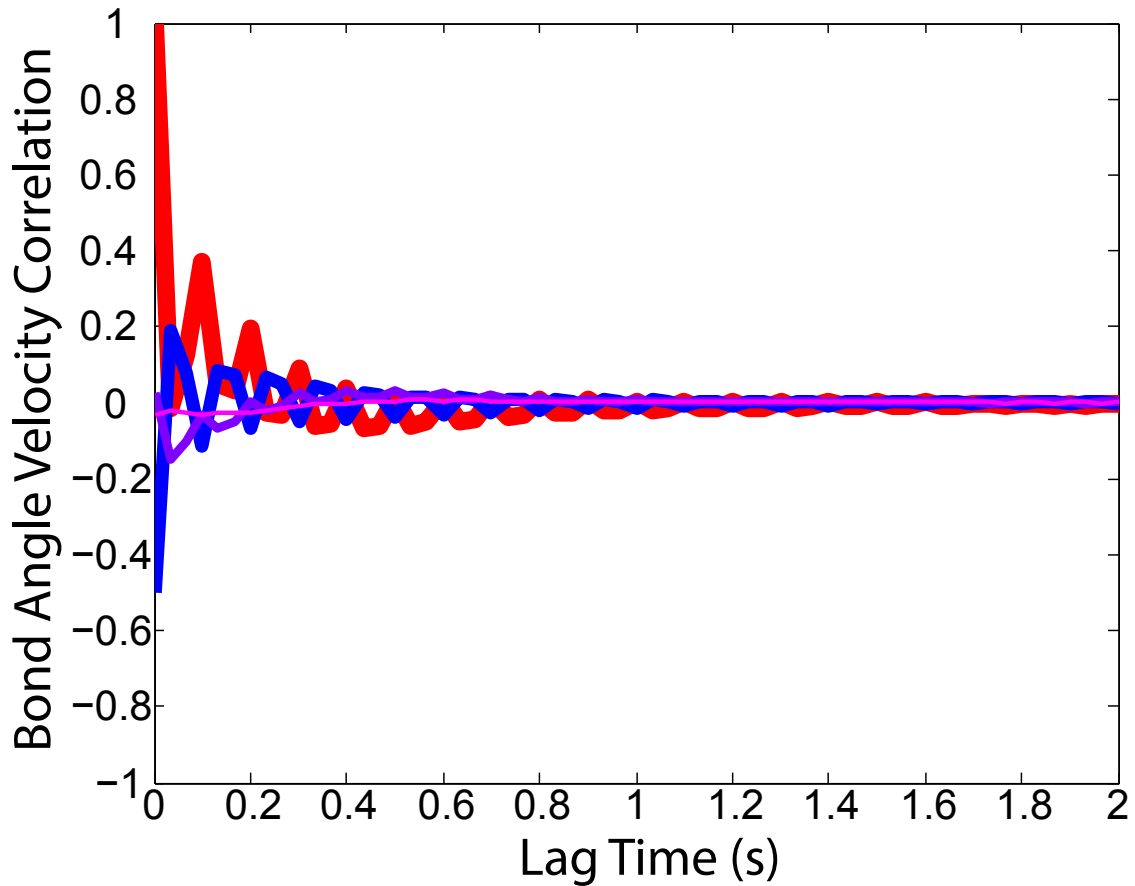


FIGURE 10. Pair Correlation Function

Average bond angle velocity autocorrelation shown in red (thickest curve) for a chain with $\alpha = \pi/6$. Nearest, second nearest, and third nearest bond angle velocity neighbor correlations shown in blue, purple, and magenta (second, third, and fourth thickest curves) respectively. The nearest neighbor bond angle velocities are initially anticorrelated due to buckling in the interconnected chain, i.e. as one bond angle is kicked its neighbor will react in the opposite direction. All correlations die off by ~ 0.3 s of lag time. The 10Hz beat frequency results from the non-commensurate dish oscillation frequency (40Hz) and imaging frequency (30Hz).

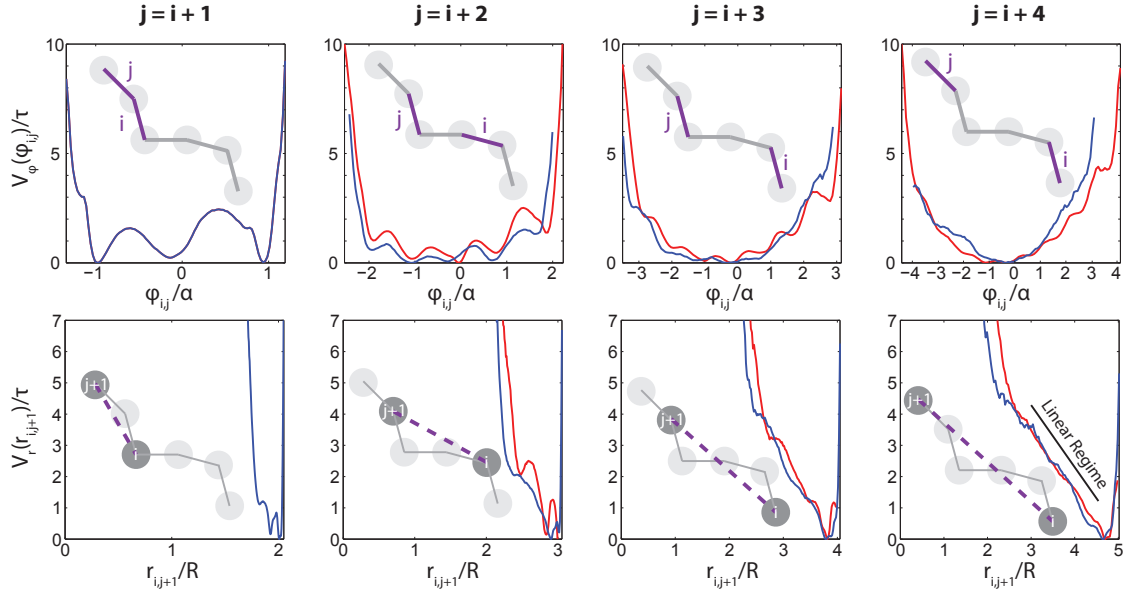


FIGURE 11. Effective Potentials

Effective potentials for total bond winding angle $\phi_{i,j}$ (top row) and interparticle distance $r_{i,j+1}$ (bottom row) with example subchains shown as inset diagrams. Potentials are determined from distributions using equations 4.3 and 4.4. The blue (dark) curves are calculated directly from empirical data and the red (light) curves are calculated using the distribution for $\phi_{i,i+1}$ to generate self-avoiding walks.

and

$$p(r_{i,j}) \propto r_{i,j} e^{-V_r(r_{i,j})/T}. \quad (4.4)$$

We show the measured effective potentials averaged over all possible sub-chains of each given length for a system with $\alpha = \pi/4$ as blue (dark) curves in Figure 11. We present similar data for $\alpha = \pi/6$ in figures 15 and 16 in chapter 6. Note that the measured potentials for both systems reach beyond $\pm\alpha$. A small amount of play was required to allow the links to slide without binding, creating a broadening of the potential. Further, water bridges form where links contacts stops creating a more complicated potential energy landscape near the boundaries. However, as we show in this paper, these details are immaterial as the variance of the nearest-neighbor bond angle distribution is all that matters in determining the physics of the system.

The winding angle potential V_ϕ is anharmonic for short chains but approaches a harmonic potential with increasing chain length, as predicted by a simple application of the renormalization group [69]. The effective potential for end-to-end distance V_r , however, does not approach a harmonic within the length of chain empirically available to us for both the $\alpha = \pi/4$ and $\pi/6$

data. This stands in contrast to the harmonic behavior expected for a freely-jointed chain, due to the fact that our chain has restrictions on bond angles and is by its nature non-intersecting. Our data are much better to match to the worm-like chain model, showing qualitatively similar end-to-end distributions (and equivalent potentials) [74].

In order to understand the behavior of these potentials for long chains we turn to simulations of our polymer. The red (light) curves in figure 11 show the effective potentials for simulated chains of the same lengths as our experimental results. The simulated data agrees with the empirical data, confirming the validity of our simulation approach.

We extrapolate to long chains in order to determine the scaling of the statistical parameters of the distributions of end-to-end distance and end-to-end winding angle. End-to-end quantities are denoted as coordinates without i, j subscripts. Figure 12 shows the scaling of the variance of end-to-end winding angle σ_ϕ^2 with N , the number of defined bond angles. We find that for sufficiently short chains, σ_ϕ^2 is linear in N . This is identical to the scaling expected for a simple random walk because at small scales self-intersections are unlikely due to the restriction of bond angles. For sufficiently long chains we find that σ_ϕ^2 exhibits a logarithmic scaling, as predicted by [71]. To determine the critical N at which chains transition between “short” and “long” we fit the data to the piecewise function

$$\sigma_\phi^2 = \begin{cases} \sigma_{\phi,0}^2 N & N < N_* \\ \sigma_{\phi,0}^2 N_* (\ln(N/N_*) + 1) & N > N_* \end{cases}. \quad (4.5)$$

where $\sigma_{\phi,0}^2$ is the already known variance of the nearest-neighbor link angle. The fit yields the value of N_* , which we find to be inversely proportional to $\sigma_{\phi,0}^2$ (Figure 12 (inset)) with a phenomenological prefactor of order 1 that is likely determined by the relative size of the particles to the links. N_* plays a similar role to a Kuhn length in a real polymer. We can collapse all of our data onto a master curve when scaled so that

$$N \rightarrow \frac{N}{N_*}, \quad \sigma_\phi^2 \rightarrow \frac{\sigma_\phi^2}{\sigma_{\phi,0}^2 N_*}. \quad (4.6)$$

We use three different families of bond angle distributions: 1) The experimentally measured distributions from our $\alpha = \pi/4$ and $\alpha = \pi/6$ systems, the corresponding potentials for which

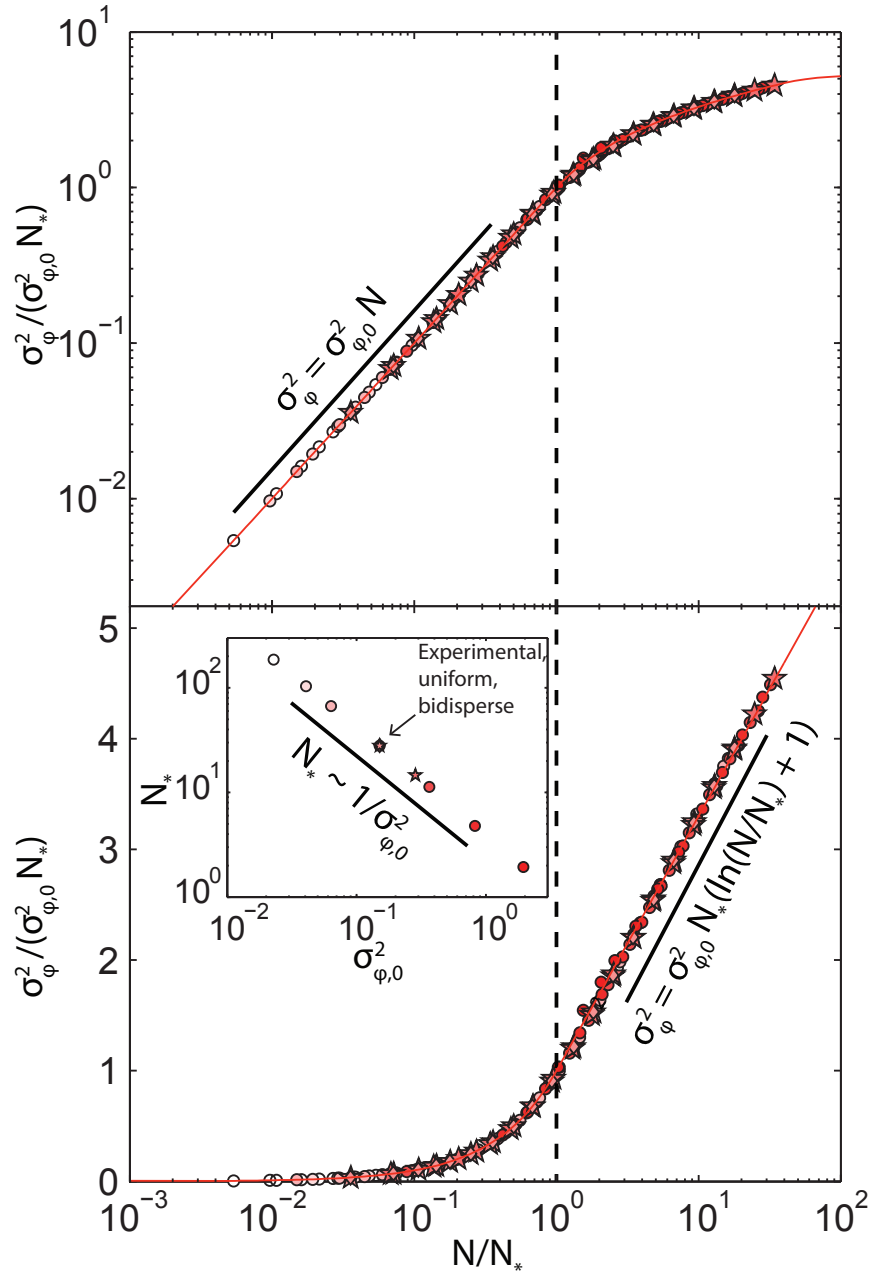


FIGURE 12. Master curves for the scaling of winding angle variance σ_ϕ^2 . The data are plotted in both log-log (top) and semilog (bottom) to illustrate power law and logarithmic scaling regimes, respectively. The shape of the markers indicates the probability distribution of nearest-neighbor link angles; stars for experimental, circles for uniform, and diamonds for bidisperse. The marker color goes from light to dark as the variance of the nearest-neighbor probability distribution increases. Equation (4.5) is plotted over the data. (inset) The critical length N_* is inversely proportional to $\sigma_{\phi,0}^2$, the variance of the nearest-neighbor link angle for a given chain.

are shown in the top left of Figure 11 and 15, respectively. 2) A uniform distribution of bond angles between $\pm\alpha$. 3) A bidisperse distribution of bond angles with value of $\pm\alpha$. We present simulational data for SAWs from uniform and bidisperse distributions tuned to have the same $\sigma_{\phi,0}^2$ as the $\alpha = \pi/6$ empirical data and find that all three associated scalings have precisely the same N_* . Thus we see that the full physics of the system is controlled by the variance of the nearest-neighbor angle distribution.

Figure 13 shows the scaling of the squared mean $\langle r \rangle^2$ and the variance σ_r^2 as a function of N . We see that all curves, for sufficiently large N , go to a power law consistent with the Flory prediction [72, 73], where

$$\langle r \rangle \sim N^\nu, \sigma_r^2 \sim N^{2\nu}, \nu = \frac{3}{4} \quad (4.7)$$

in two dimensions. We collapse all of our data onto a master curve for $N \gg N_*$ by scaling $N \rightarrow N/N_*$ and

$$\langle r \rangle^2 \rightarrow \frac{\langle r \rangle^2}{(C_1 + C_2)N_*^{3/2}}, \sigma_r^2 \rightarrow \frac{\sigma_r^2}{(C_1 + C_2)N_*^{3/2}} \quad (4.8)$$

where the constants C_1 and C_2 are fitted prefactors (figure 13). This scaling was selected such that $\langle r^2 \rangle = \langle r \rangle^2 + \sigma_r^2 = 1$ at $N = N_*$, preserving relative magnitude of both statistical parameters.

Our simulations show that the for lengths much longer than experimentally accessible the radial potentials eventually become harmonic as expected (Figure 17 in chapter 6). However, for short and intermediate lengths the curves show non-trivial behavior. The compression stiffness of the polymer, which is related inversely to the variance in end-to-end distance, is far higher in short chains than would be predicted by the Flory power law. As these chains grow, the stiffness necessarily softens very rapidly in order to meet the long chain limit and match expectations above the crossover from “short” to “long.”

Our system shows clear hallmarks of semiflexibility [74, 75], with the end-to-end potential transitioning from a rigid state in which the equilibrium position is near full extension of the chain, to a flexible state with an equilibrium position near zero (Figure 17 in chapter 6). We see further evidence of semiflexibility in the existence of a linear regime in our experimentally determined potentials (Figure 11, lower right). In the intermediate lengths between the two states, the potential temporarily becomes wide and flat before becoming harmonic. This intermediate-scale widening explains the rapid scaling of the variance at these lengths. This roll-

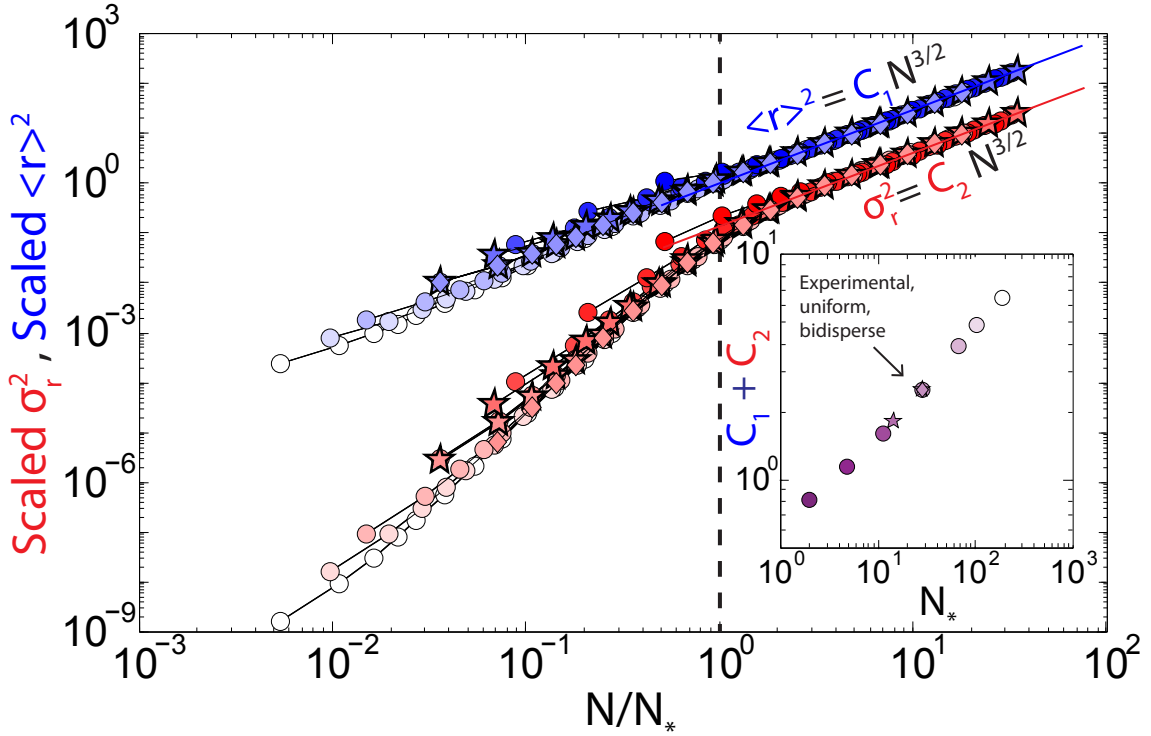


FIGURE 13. Scaling Laws for End-to-End Distance

Scaling of variance in end-to-end distance σ_r^2 (lower curve) and squared mean of end-to-end distance $\langle r \rangle^2$ (upper curve). The shape and color of the markers indicates the probability distribution of nearest-neighbor bond angles as in figure 12. Both curves are scaled by a factor of $(C_1 + C_2)N_*^{3/2}$, where N_* is the same critical length from figure 12, and collapse to $N^{3/2}$ power laws for $N \gg N_*$. (inset) The sum of scaling coefficients C_1 and C_2 plotted against critical length N_* .

over phenomenon is a result of our bonds being treated as rigid rods. This assumption is valid as considering only torsional degrees of freedom is a standard in the field, consistent with the rotational isomeric state model of polymers [76, 77].

Conclusion

In this study we have presented a simple mechanical analog to short chain molecules. We see that the effective interaction potential for winding angle quickly becomes harmonic as chain length increases, despite the decidedly non-harmonic nearest-neighbor interaction. Though the effective potential for end-to-end distance does not become harmonic over the length of our empirical chain, we are able to extrapolate for considerably longer chains and show that it eventually assumes the familiar Hookean form. We show that our system may be treated as

a self-avoiding walk with scalings that are consistent with [71] and [72, 73] in the long-chain limit and that the full character of these scalings is determined by the width of the nearest-neighbor bond angle distribution. We show that short- and intermediate-length chains exhibit unconventional behavior, a result likely connected to the relative rigidity of bond lengths. Ultimately, we demonstrate that over the full range of lengths studied all of the physics is controlled by the variance of the nearest neighbor bond-angle distribution.

Our simulation method accurately predicts the behavior of our mechanical system at the short scale as well as the well-known behavior of polymers in the long-chain limit. Therefore, our mechanical analog is consistent with polymer physics and may be used to speak to the non-universal mechanics of short chain molecules. Our macroscopic, mechanical system is uniquely suited to passively study these lengths as we can build the physics from the bottom up all while operating at easily observable length and time scales. It is remarkable that such a simple macroscopic analog can point to a better understanding of the constitutive mechanics of microscopic polymers. Beyond the study of polymers, the relative link angles in our chain can be mapped as spins onto a 1D lattice, so this experiment can be viewed as a simple mechanical simulation of a 1D X-Y model with peculiar nearest neighbor interactions.

CHAPTER V

DETAILED MATERIALS AND METHODS FOR CHAPTER 3

Shaker Assembly

The waves are generated in a water-filled aluminum dish (diameter 17.5 inches, depth 0.5 inches) that is vertically oscillated with RMS amplitude A_s and at frequency f_s (Fig. 5(a) in chapter 3). The dish is mounted on a ceramic-coated aluminum shaft (diameter 2 inches), which passes through a 2 inch inner diameter air bushing (New Way Air Bearings). This assembly is leveled by a stage mounted to the outside of the bushing mounting block. The ceramic-coated shaft is connected by a 24 inch length of 1 inch T-slot framing to an electromechanical shaker (Vibration Test Systems VTS-100) controlled by a digital function generator (Stanford Research Systems Model DS335) through a voltage amplifier (Behringer Europower EP4000). Four springs connect the T-slot framing shaft to the external armature, bearing nearly all of the static load. An accelerometer is mounted to the bottom of the dish to measure stroke amplitude and frequency through a digital oscilloscope (Tektronix TDS 2012C).

Rheometer

The driving arm of the rheometer is laser-cut from acrylic and has attached to it two neodymium magnets (K&J Magnetics, cylinder magnets; thickness 0.125 in, diameter 0.5 in, moment $m_1 = 0.42 \text{ A m}^2$). Each magnet is positioned $R = 3\text{cm}$ from the the center of the arm with their north poles up. The driving arm sits at the end of a long aluminum shaft and is rotated about its center by a stepper motor driven by an Arduino Uno. The long shaft ensures that there is no effect due to magnetic interactions with the stepper motor. The test rotor consists of two closed-cell nylon foam disk floats held at the same $R = 3\text{cm}$ from the center as the driving arm magnets by a laser cut piece of balsa wood. The wood piece has a hole in its center which, when slipped over a delrin post set into the center of the dish, holds the test rotor coaxial with the driving arm but free to rotate. In the center of each float disk is a neodymium magnet (K&J Magnetics, cylinder magnets; thickness 0.0625 in, diameter 0.25 in, moment $m_2 = 0.053 \text{ A m}^2$) with its north pole up. The vertical separation between the driving arm and the test rotor is $h = 6\text{cm}$. A contactless magnetic encoder (Avago Technologies, part number AEAT-6600-T16) is

used to track the angular position of the test particle. To facilitate this a cylindrical, diametric (polarization orthogonal to the axis of symmetry) magnet with an axial pass-through hole is mounted in the center of the wooden connector. The magnetic encoder is mounted on top of the center post and is recorded by a second Arduino Uno.

Derivation of Torque Due to Magnets

Here we derive, in exact form, the torque on the test rotor as a function of relative angle γ .

We begin by defining all salient parameters and variables. Figs. 5(a) and (b) illustrate the relationship between the quantities.

- θ : Angular position of the test rotor
- γ : Relative angle between the drive arm and test rotor when viewed from above
- R : distance of the magnets from the axis of rotation
- $\vec{m}_1 = m_1\hat{z}$ and $\vec{m}_2 = m_2\hat{z}$: magnetic moments of the upper and lower magnets, respectively
- \vec{r} : separation of the upper magnet from the lower magnet
- a : lateral distance between the upper and lower magnets (defining the \hat{x} direction)
- h : vertical distance between the upper and lower magnets

The coordinates and dimensions of the system are related to one another as

$$r = \sqrt{h^2 + a^2} = \sqrt{h^2 + 4R^2 \sin^2\left(\frac{\gamma}{2}\right)}. \quad (5.1)$$

Given that $\vec{m}_1 = m_1\hat{z}$, $\vec{m}_2 = m_2\hat{z}$ and $\vec{r} \cdot \hat{z} = h$, the force between the upper and lower magnets is

$$\vec{F}(\vec{r}, \vec{m}_1, \vec{m}_2) = \frac{3\mu_o m_1 m_2}{4\pi r^5} \left(2h\hat{z} + \left(1 - \frac{5h^2}{r^2}\right) \vec{r} \right). \quad (5.2)$$

The exerted in-plane torque is driven by the component of the force that is directed tangent to the arc of rotation. To obtain this, we first find the \hat{x} component of \vec{F} which lies along a . Noting that $\vec{r} \cdot \hat{x} = a$, we can write down the \hat{x} component of \vec{F} as

$$F_x = \vec{F} \cdot \hat{x} = \frac{3\mu_o m_1 m_2 R}{2\pi r^5} \left(1 - \frac{5h^2}{r^2}\right) \sin\left(\frac{\gamma}{2}\right). \quad (5.3)$$

We calculate the component of the force tangent to the arc of rotation $F_\gamma = F_x \cos(\frac{1}{2}\gamma)$ and thus the torque $\tau = F_\gamma R$ using the identity $\sin(\frac{1}{2}\gamma) \cos(\frac{1}{2}\gamma) = \frac{1}{2} \sin \gamma$ to obtain

$$\tau(\gamma) = \frac{3\mu_o m_1 m_2 R^2}{2\pi} \left(\frac{1}{r^5} - \frac{5h^2}{r^7} \right) \sin \gamma. \quad (5.4)$$

This is the exact form for the torque on the test particle as a function of relative angle γ , with an extra factor of 2 to account for the fact that our system has two pairs of magnets. For simplicity, we would like to approximate this as a Hookean torque. To do this, we make the approximation that $r \approx h$ and $\sin \gamma \approx \gamma$. This is a small-angle approximation, and will break down as γ increases. The Hookean torque we obtain is

$$\tau(\gamma) = -k_r \gamma \quad (5.5)$$

where

$$k_r = \frac{6\mu_o m_1 m_2 R^2}{\pi h^5}. \quad (5.6)$$

For the particular parameters of our system, $k_r \approx 6 \times 10^{-5}$ Nm. Fig. 14 shows the torque in exact form and the linear approximation over a range of relevant angles.

Measurement of Drag Coefficient

We program the driving arm's position β to oscillate sinusoidally as

$$\beta(t) = \beta_0 \sin(\omega t), \quad (5.7)$$

where β_0 is the oscillation amplitude and ω is the angular driving frequency. Assuming a well defined coefficient of drag, the resulting motion of the test particle is described by the differential equation

$$I\ddot{\theta} = \tau(t) - \zeta_r \dot{\theta}, \quad (5.8)$$

where θ is the angular position of the test particle, I is the the moment of inertia, $\tau(t)$ is the torque applied by the driving arm and ζ_r is the rotational drag coefficient. The applied torque τ is only dependent on the relative angle $\gamma(t) = \theta(t) - \beta(t)$ between the driving arm and the test particle, and so can be parameterized as $\tau(t) = \tau(\gamma(t))$. We derive the exact form of this torque

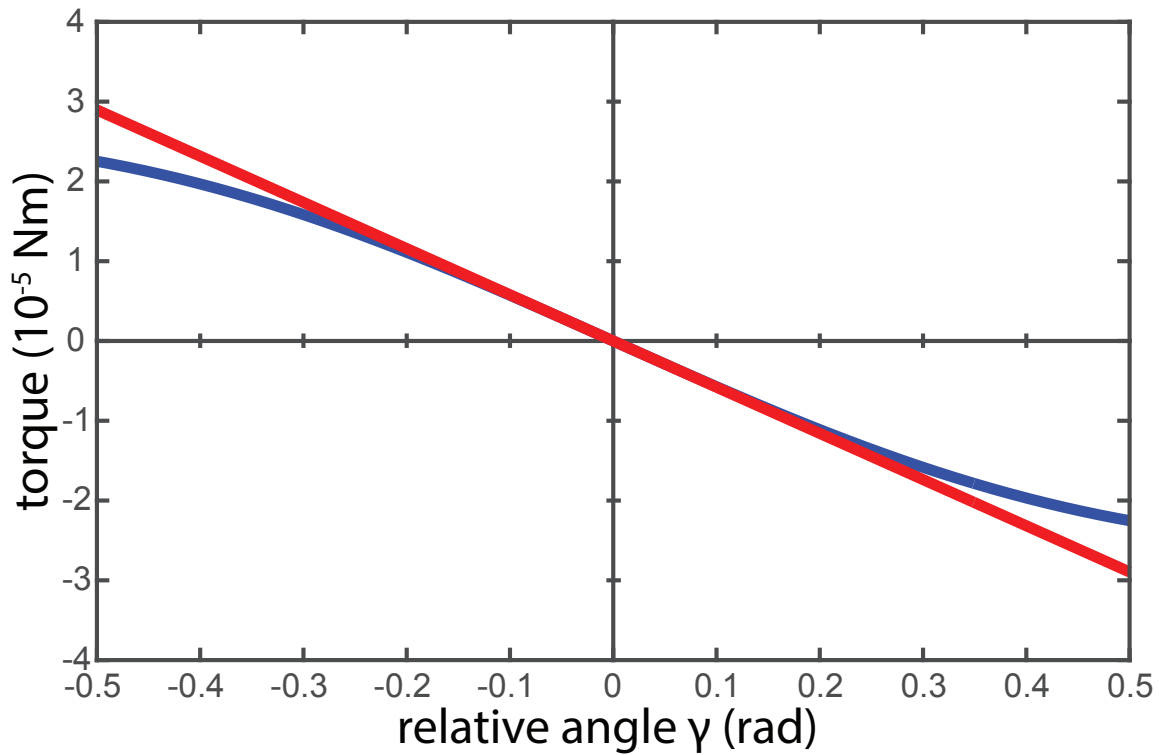


FIGURE 14. Comparison of Hookean approximation and full form for torque exerted by drive arm

The full form torque (blue) is well approximated by a Hookean torque with spring constant $k_r \approx 6 \times 10^{-5} \text{Nm}$ (red) over a range of angles relevant to our active measurement of drag coefficient.

above and find that it is well approximated by a Hookean spring:

$$\tau(\gamma) = -k_r \gamma, \quad (5.9)$$

with spring constant

$$k_r = \frac{6\mu_0 m_1 m_2 R^2}{\pi h^5} \approx 6 \times 10^{-5} \text{ Nm}. \quad (5.10)$$

Here, m_1 and m_2 are the magnitudes of the magnetic moments of the driving arm and test particle magnets, respectively. This approximation allows us to solve equation 5.8 exactly as a damped driven harmonic oscillator to find

$$\theta(t) = \theta_0 \sin(\omega t + \phi), \quad (5.11)$$

where

$$\theta_0 = \beta_0 \frac{k_r}{I \omega Z_m(\omega)}, \quad (5.12)$$

the mechanical impedance is

$$Z_m(\omega) = \sqrt{\left(\frac{\zeta_r}{I}\right)^2 + \frac{1}{\omega^2} \left(\frac{k_r}{I} - \omega^2\right)^2}, \quad (5.13)$$

and the phase lag is

$$\phi(\omega) = \tan^{-1} \left(\frac{\zeta_r}{I} \frac{\omega}{\omega^2 - \frac{k_r}{I}} \right). \quad (5.14)$$

We solve for the drag coefficient to find

$$\zeta_r = \frac{k_r \beta_0}{\omega \theta_0} \sin \phi. \quad (5.15)$$

Thus, we are able to calculate the drag coefficient by measuring the amplitude and phase lag of the test rotor's response relative to the the driving signal. We obtain the response amplitude and phase lag using a simple lock-in measurement:

$$\theta_0 = \left(\langle \theta(t) \cos(\omega t) \rangle^2 + \langle \theta(t) \sin(\omega t) \rangle^2 \right)^{1/2}, \quad (5.16)$$

$$\phi = \tan^{-1} \left(\frac{\langle \theta(t) \sin(\omega t) \rangle}{\langle \theta(t) \cos(\omega t) \rangle} \right), \quad (5.17)$$

where the angle brackets indicate time averages.

CHAPTER VI

SUPPLEMENTARY MATERIALS FOR CHAPTER 4

Effective Potentials for Chain With $\alpha = \pi/6$

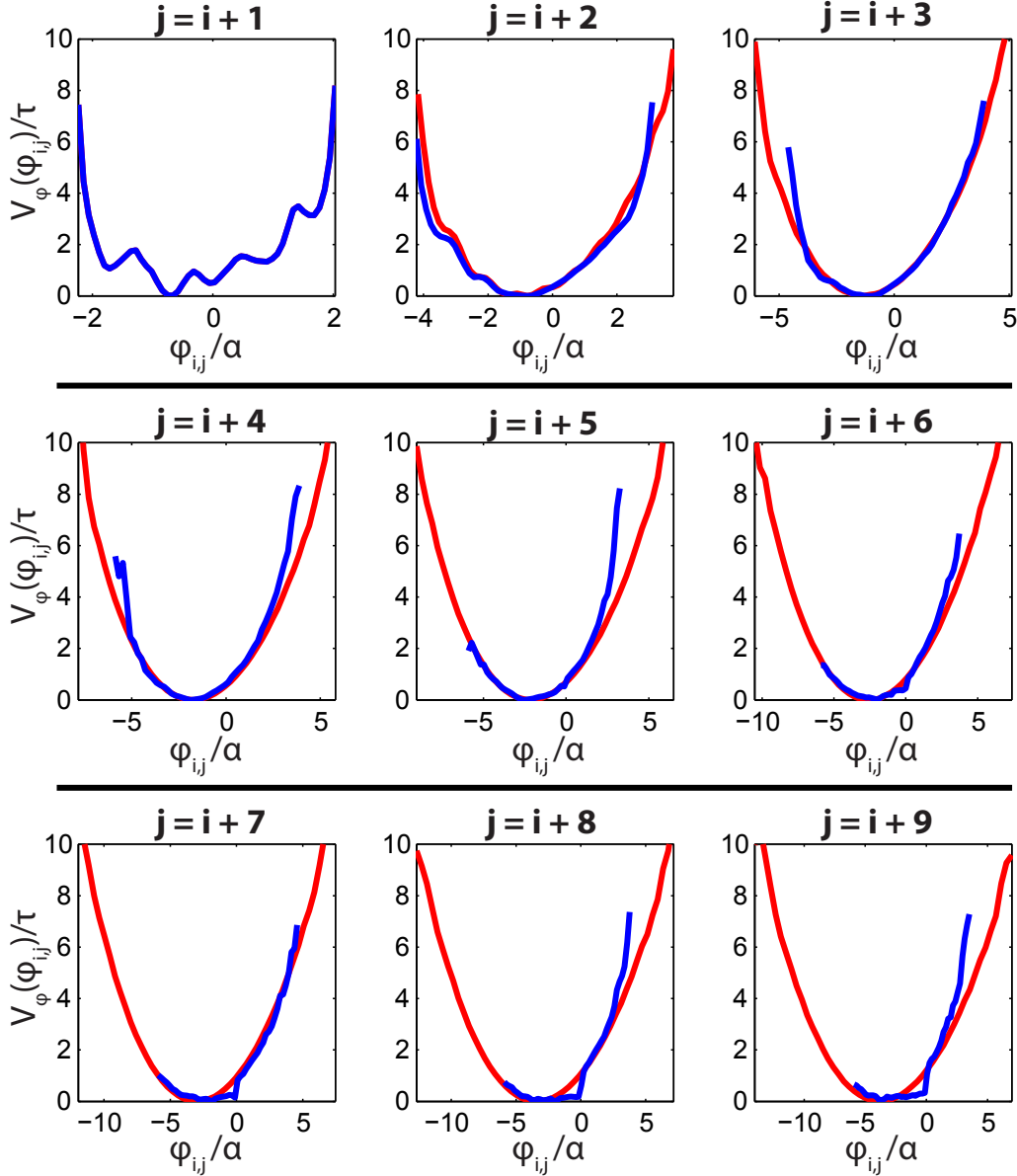


FIGURE 15. Effective Potentials in Total Bond Winding Angle $\phi_{i,j}$
 Potentials are determined from distributions using equation 3. The blue curves are calculated directly from empirical data and the red curves are calculated using the distribution for $\phi_{i,i+1}$ to generate self-avoiding walks.

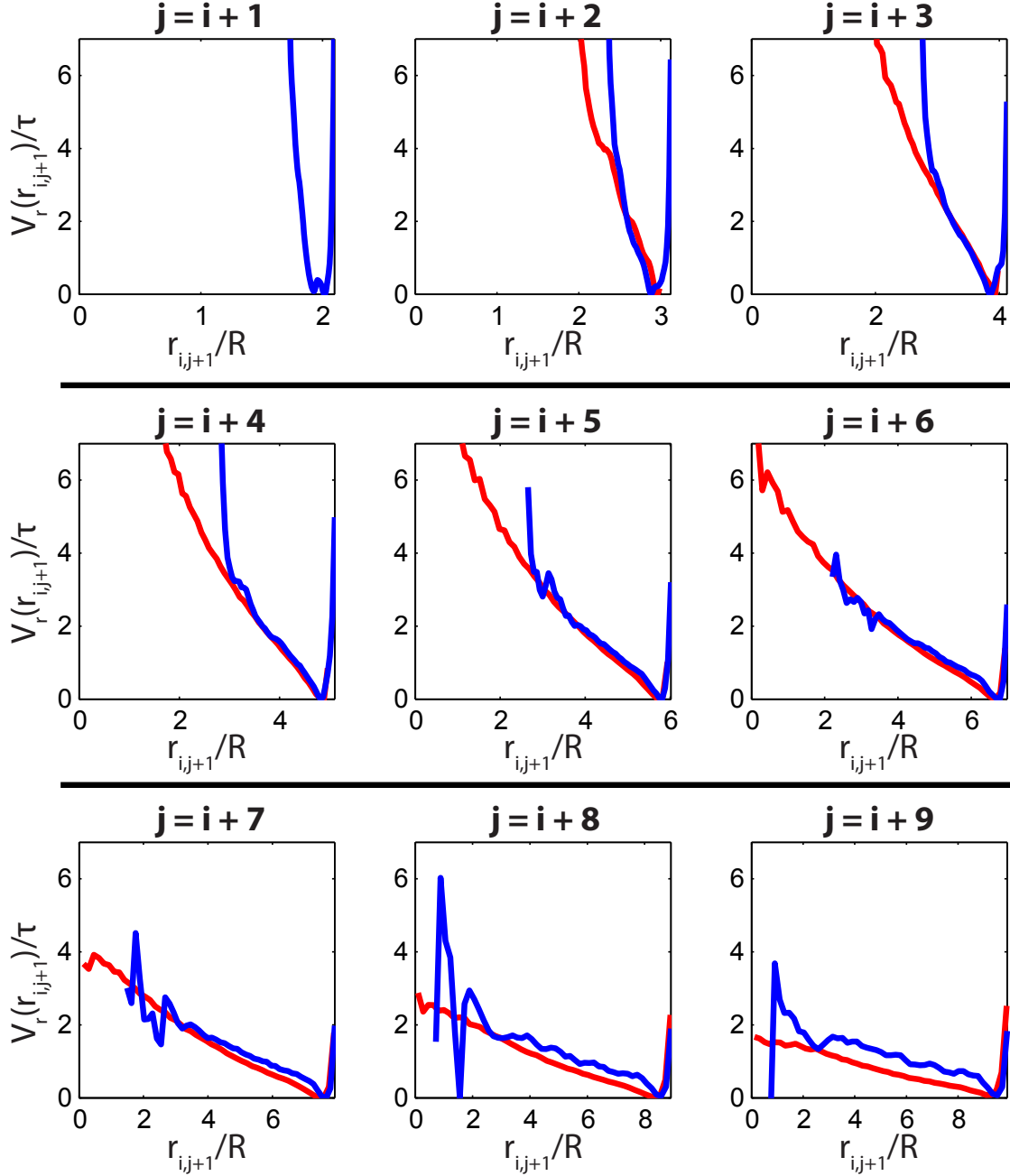


FIGURE 16. Effective potentials for interparticle distance $r_{i,j+1}$. Potentials are determined from distributions using equation 4. The blue curves are calculated directly from empirical data and the red curves are calculated using the distribution for $\phi_{i,i+1}$ to generate self-avoiding walks.

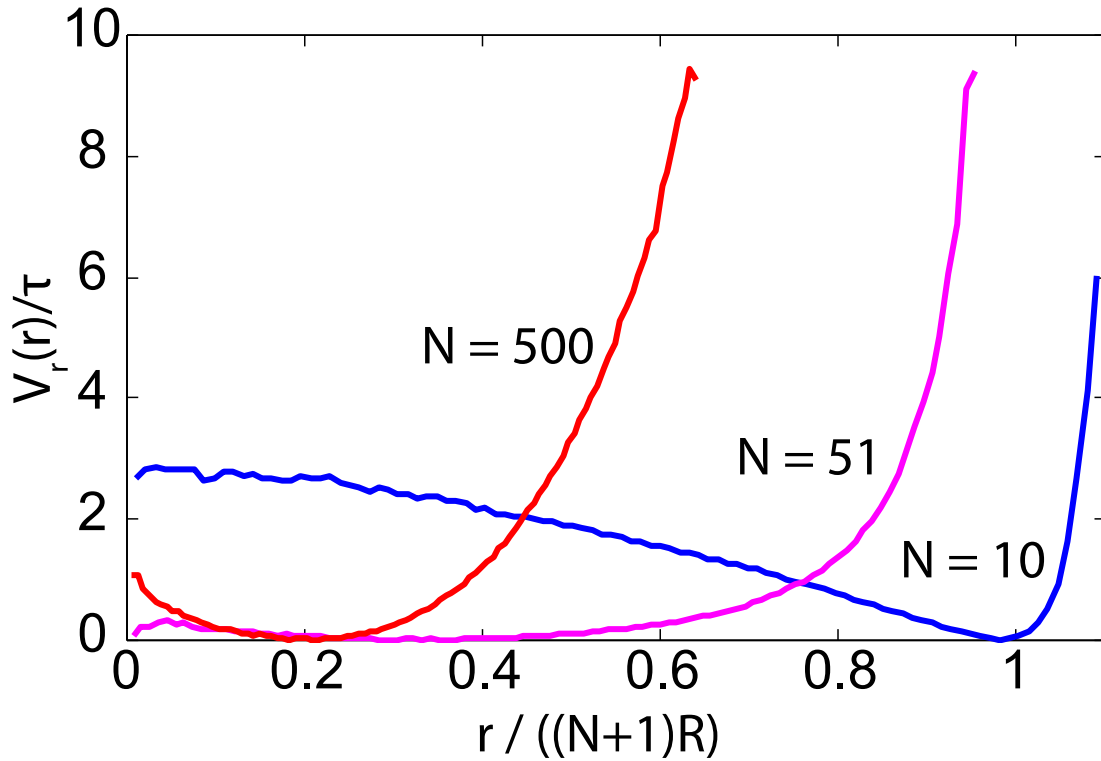


FIGURE 17. Extrapolated Effective Potentials for End-to-End distance of Long Chains Shown is the crossover from rigid behavior (anharmonic) at low N to flexible behavior (harmonic) at high N .

Semiflexible Behavior

Self avoiding walk simulation algorithm

We create self avoiding random walks with fixed bond length $22m$, particle diameter $15mm$ and bond angles $\phi_{i,i+1}$ drawn from a given predefined distribution $P(\phi_{i,i+1})$. In order to build a chain with N bond angles we employ the following algorithm:

Begin

Draw N bond angles from the distribution

For each particle

Calculate the (x,y) value

Test for intersection with all previous particles and links

EndFor

Repeat until a chain of N non-intersecting links is found

CHAPTER VII

CONCLUSION

This work establishes chaotic Faraday waves as a metafluid that a) is wholly consistent with equilibrium thermal physics, b) has independently tunable temperature and viscosity and c) provides a new platform on which complex, many-body phenomena may be studied. It hints at a new universality: systems need only meet the basic criteria of having steady-state and isotropic chaos to be governed by the fundamental physics of equilibrium thermodynamics. This work opens up a new set of exciting questions and applications to be addressed in future work.

Chapter 2 established the system of chaotic surface waves as a thermal-like fluid composed of macroscopic elements, based on passive rheology of buoyant tracers. The motion of passive tracer particles exhibits a clear crossover from ballistic to diffusive motion. This motion is functionally identical to Brownian motion, differing only in length and timescales. This scale difference is the utility of the system; it dilates the constitutive dynamics to easily observable levels, where complicated optics and imaging setups are not required to obtain detailed quantitative data. I showed how, from passive tracer motion, one is able to measure the temperature of the chaotic waves. I also determined how this temperature depends on the external driving parameters, in particular, that it is directly proportional to the amplitude of the vertical agitation generating the waves. Further, I showed that the *inferred* viscous drag coefficient (calculated using the temperature and diffusion constant and by *assuming* the Einstein relation in our system) is consistent with what would be expected in a nearly ideal gas.

Chapter 2 also begins the discussion of applying equilibrium thermal physics to ostensibly athermal or non-equilibrium systems. The chaotic waves are far from what would be traditionally considered thermal or equilibrium: they are macroscopic, and their dynamics do not depend on the room temperature, making them athermal with respect to their surroundings. The waves are also indisputably non-equilibrium, as their existence depends on the input of energy in the form of vertical agitation. Nevertheless, they seem to satisfy the basic criteria of kinetic theory in having steady-state, isotropic chaos. Chapter 2 showed that chaotic Faraday waves are, at the very least, consistent with an equilibrium thermal fluid, and that they have a well-defined and easy-to-control temperature. The results however lack a key piece: a direct measure of viscous drag.

Chapter 3 addresses this deficiency by introducing an active rheology of chaotic Faraday waves. Here, by applying a sinusoidally varying torque to a test rotor, I demonstrated the measurement of a viscous drag coefficient. This “closes the loop” left open by chapter 2. With direct measurement of temperature, diffusion constant and drag coefficient in the chaotic waves I showed that this system does in fact obey the Einstein relation, a fundamental result of equilibrium thermodynamics. This validated our assumptions regarding the thermal-like nature of chaotic Faraday waves. This now leads to broader implications: perhaps, so long as the fundamental units of a system exhibit isotropic, steady-state chaos, the system can be treated with the same physics as an equilibrium thermal system. This suggests that equilibrium thermodynamics may be extended to certain classes of otherwise non-equilibrium or athermal systems, or, put another way, that equilibrium thermodynamics may be more universal than previously thought.

Chapter 3 also showed the systematic dependence of the viscous drag coefficient on input parameters. The viscous drag imparted by the chaotic waves is proportional to the product of the vertical driving amplitude and frequency. Considering again that the temperature of the waves is proportional only to the vertical driving amplitude, this now shows that chaotic Faraday waves form a fluid that has *independently* tunable viscosity and temperature. This is a remarkable property because in conventional fluids, there exists a strict relationship between viscosity and temperature. Here, no such restriction exists. Instead, this fluid need only obey the Einstein relation but is otherwise free to move about the temperature-diffusion constant-viscous drag coefficient phase space. Additionally, my analysis showed that the drag coefficient was independent of particle velocity, meaning that, for the range of parameters relevant to my experiment, the chaotic Faraday waves are a Newtonian fluid.

When taken together, chapters 2 and 3 demonstrate that chaotic Faraday waves may be considered a thermal, Newtonian, tunable metafluid. I call this system a metafluid because it is constructed using the same philosophy behind all metamaterials: replacing atoms and molecules with larger, athermal (with respect to the room or bath temperature) elements as the fundamental unit from which emergent material properties are derived. While there is still work to be done in rigorously characterizing the chaotic Faraday waves as a thermal metafluid, we may still use it as a novel platform on which to study analogs to complex microscopic phenomena.

Chapter 4 shows one such application. Here, I constructed buoyant articulated chains as macroscopic analogs to short-chain polymers and placed them in the chaotic Faraday waves. This demonstrated the utility of the waves as a source of thermal agitation. Whereas in a microscopic system, a polymer is allowed to explore its configurational space through random collisions with the surrounding atoms and molecules, instead my polymer analog is allowed to explore its configurational space through collisions with macroscopic chaotic wave excitations. My analysis shows that, strikingly, these macroscopic polymer analogs are still entirely consistent with the well-studied physics of real polymers.

Again, the utility of the chaotic wave system is in its scale. Whereas monomer-level behavior must be inferred from bulk behavior in molecular systems, here we may observe the dynamics of the polymer from the monomer scale up to the chain scale. This suggests that this system will be able to shed light on other microscopic phenomena that occur at length and/or time scales too small to easily observe.

There are many other applications that may be pursued in the future. The most tempting is the study of many-particle phenomena. For example, buoyant particles with similar hydrophobicity tend to attract on the surface of a fluid via the popularly-termed “Cheerios effect,” after the way Cheerios tend to clump together on the surface of milk [78]. This leads to passive aggregation of buoyant particles at the air-water interface. At several points during my graduate career I have taken exploratory forays into many-particle problems. Though I have not achieved any powerful quantitative results, I have made several qualitative observations that I believe point to the potential for impactful science. For example, if many uniform particles are placed in the chaotic Faraday waves, they will tend to anneal into crystal structures at low shaker amplitudes. At higher amplitudes (and thus higher temperature of the chaotic waves), small crystalline clusters will sublime into a gas-like state of free particles. Thus, we may observe each individual particle in a material as it undergoes a phase transition. A serious systematic difficulty arises for large clusters, however, in that the dense packing of particles in the center of a cluster damps out the surface waves, effectively lowering the internal temperature of the cluster to our system’s absolute zero (the point at which there are no chaotic waves). Nevertheless, I believe that through careful design of experiments the chaotic Faraday wave system will prove to be a powerful tool in studying phase transitions.

Another future direction for this work is to examine self-assembly and pattern formation. Self-assembly is an active and exciting area of research [51], with applications to both inorganic nanotechnology [79] and biology [80, 81]. In fluid interface systems, the Cheerios effect can in fact be tuned via particle hydrophobicity and shape. Theoretically, buoyant particles could be designed to bind to or repel from one another with preferred orientations, self-assembling into larger, more complex macrostructures. For example, the chains of particles described in chapter 4 could be modified to be heterogenous, leading them to self-fold into particular structures. The Faraday waves provide an element of thermal agitation that allow particles to passively explore their state space and anneal into their optimal structure.

There are a number of directions future researchers may carry this work in addition to the aforementioned applications. To begin with, there are deeper characterization yet to try in the chaotic Faraday waves. My research has focused on the use of tracer particles. We find that the *tracers* diffuse identically to thermal particles, but we do not say anything about the waves themselves. One possible method to study any diffusive nature of the waves would be to perform a scattering-style experiment, similar to those used to study diffusive dynamics in colloidal glasses [82]. The method is relatively simple: image the waves at a frequency commensurate with that of the shaker, and examine the spatial correlations of the waves for frames separated by various lag times. The decay constant of these correlations can be used to determine if the waves themselves are diffusive or not.

We have demonstrated many canonical results of equilibrium thermodynamics with this work, but there are many more out there. Do the laws of thermodynamics exist in our system? For example, can we recover a zeroth law? To answer this question, one would need to demonstrate energy transport between two coupled chaotic Faraday wave systems. This could be accomplished by embedding test rotors in each of two systems and couple the rotors via electromechanical means. If the two baths are held at constant but different temperatures, a zeroth law of thermodynamics would result in a measurable energy flux travelling from the probe in the hotter reservoir to the probe in the colder reservoir. A similar experiment has already been performed in a granular gas system [83] and indeed confirmed that energy flows from hot to cold in accordance with the notion of irreversibility, at a rate proportional to the temperature difference between the baths. Not only does this previous work show a proof-of-concept for how

one might measure the thermodynamics of a macroscopic, non-equilibrium system, it also once again points toward a broader universality of thermal physics.

I have helped design an experiment in our lab that is still in its infancy to probe this notion of universality. I have proposed that we build a granular gas system and extract from it thermal behavior in the same way we have in the Faraday waves. Granular gasses are not a new system for study [84], but I have proposed a new form of agitation. Granular gasses are generally created by shaking grains or blowing air through them, often from beneath. This is an efficient way for achieving the desired gas-like phase, but it inherently introduces anisotropy, thus leading it away from the traditional tools of thermal physics. The system I have proposed uses isotropic, turbulent (chaotic) air input as a means of fluidization for a two-dimensional granular gas. The goal of the project, though I will no longer be present to see it through, is to once again attempt to recover the Einstein relation in the gas just as we did in the chaotic Faraday waves. If the same physics emerges, we will have two examples of macroscopic, non-equilibrium systems that exhibit behavior consistent with equilibrium thermal systems, despite satisfying only the basic criteria of steady-state chaos and isotropy. A successful result will lend further support to the notion that thermodynamics may be more universal than previously thought.

I began this dissertation by saying that materials science is a lot like cooking. We do our best to understand the ingredients, then we mix them together to make new, interesting things. The properties of the new things must necessarily be determined by the properties of the ingredients. When baking a cake, it used to be said that “there’s no substitute for an egg.” We now know that to be false; all it took was experimentation. I believe my work parallels this sentiment. Thermodynamics has been traditionally applied to microscopic systems, but that tradition does not preclude a broader universality. By stripping the physics down to bare fundamentals, we have found that macroscopic systems can reproduce equilibrium thermal behavior, and in so doing we have found a substitute for the proverbial egg.

REFERENCES CITED

- [1] D. R. Smith, J. B. Pendry, and M. C. K. Wiltshire. Metamaterials and Negative Refractive Index. *Science*, 305(5685):788–792, August 2004. ISSN 0036-8075, 1095-9203. doi: 10.1126/science.1096796. URL <http://www.sciencemag.org/content/305/5685/788>.
- [2] Kosmas L. Tsakmakidis, Allan D. Boardman, and Ortwin Hess. ‘Trapped rainbow’ storage of light in metamaterials. *Nature*, 450(7168):397–401, November 2007. ISSN 0028-0836. doi: 10.1038/nature06285. URL <http://www.nature.com/nature/journal/v450/n7168/full/nature06285.html>.
- [3] Jason Valentine, Shuang Zhang, Thomas Zentgraf, Erick Ulin-Avila, Dentcho A. Genov, Guy Bartal, and Xiang Zhang. Three-dimensional optical metamaterial with a negative refractive index. *Nature*, 455(7211):376–379, September 2008. ISSN 0028-0836. doi: 10.1038/nature07247. URL <http://www.nature.com/nature/journal/v455/n7211/full/nature07247.html>.
- [4] Zhengyou Liu, Xixiang Zhang, Yiwei Mao, Y. Y. Zhu, Zhiyu Yang, C. T. Chan, and Ping Sheng. Locally Resonant Sonic Materials. *Science*, 289(5485):1734–1736, September 2000. ISSN 0036-8075, 1095-9203. doi: 10.1126/science.289.5485.1734. URL <http://www.sciencemag.org/content/289/5485/1734>.
- [5] Thomas Brunet, Jacques Leng, and Olivier Mondain-Monval. Soft Acoustic Metamaterials. *Science*, 342(6156):323–324, October 2013. ISSN 0036-8075, 1095-9203. doi: 10.1126/science.1241727. URL <http://www.sciencemag.org/content/342/6156/323>.
- [6] Roman Süssstrunk and Sebastian D. Huber. Observation of phononic helical edge states in a mechanical topological insulator. *Science*, 349(6243):47–50, July 2015. ISSN 0036-8075, 1095-9203. doi: 10.1126/science.aab0239. URL <http://www.sciencemag.org/content/349/6243/47>.
- [7] Jesse L. Silverberg, Arthur A. Evans, Lauren McLeod, Ryan C. Hayward, Thomas Hull, Christian D. Santangelo, and Itai Cohen. Using origami design principles to fold reprogrammable mechanical metamaterials. *Science*, 345(6197):647–650, August 2014. ISSN 0036-8075, 1095-9203. doi: 10.1126/science.1252876. URL <http://www.sciencemag.org/content/345/6197/647>.
- [8] Scott Waitukaitis, Rémi Menaut, Bryan Gin-ge Chen, and Martin van Hecke. Origami Multistability: From Single Vertices to Metasheets. *Physical Review Letters*, 114(5):055503, February 2015. doi: 10.1103/PhysRevLett.114.055503. URL <http://link.aps.org/doi/10.1103/PhysRevLett.114.055503>.
- [9] Jesse L. Silverberg, Jun-Hee Na, Arthur A. Evans, Bin Liu, Thomas C. Hull, Christian D. Santangelo, Robert J. Lang, Ryan C. Hayward, and Itai Cohen. Origami structures with a critical transition to bistability arising from hidden degrees of freedom. *Nature Materials*, 14(4):389–393, April 2015. ISSN 1476-1122. doi: 10.1038/nmat4232. URL <http://www.nature.com/nmat/journal/v14/n4/full/nmat4232.html>.
- [10] Peter J Rankin, John M Ginder, and Daniel J Klingenberg. Electro- and magneto-rheology. *Current Opinion in Colloid & Interface Science*, 3(4):373–381, August 1998. ISSN 1359-0294. doi: 10.1016/S1359-0294(98)80052-6. URL <http://www.sciencedirect.com/science/article/pii/S1359029498800526>.

- [11] Ryotaro Ozaki, Masashi Aoki, Katsumi Yoshino, Kohji Toda, and Hiroshi Moritake. Effective viscosity for nematic-liquid-crystal viscosity measurement using a shear horizontal wave. *Physical Review E*, 81(6):061703, June 2010. doi: 10.1103/PhysRevE.81.061703. URL <http://link.aps.org/doi/10.1103/PhysRevE.81.061703>.
- [12] Michael Faraday. On a peculiar class of acoustical figures; and on certain forms assumed by a group of particles upon vibrating elastic surfaces. *Philosophical Transactions of the Royal Society*, 121:299–318, 1831.
- [13] L. Rayleigh. On the crispations of fluid resting upon a vibrating support. *Phil. Mag*, 16(5): 50–58, 1883.
- [14] Ludwig Boltzmann. *Weitere Studien über das Wärmegleichgewicht unter Gasmolekülen*. Wien, 1872.
- [15] Kyle J. Welch, Isaac Hastings-Hauss, Raghuvveer Parthasarathy, and Eric I. Corwin. Ballistic and diffusive dynamics in a two-dimensional ideal gas of macroscopic chaotic Faraday waves. *Physical Review E*, 89(4):042143, April 2014. doi: 10.1103/PhysRevE.89.042143. URL <http://link.aps.org/doi/10.1103/PhysRevE.89.042143>.
- [16] Kyle J. Welch, Clayton S. G. Kilmer, and Eric I. Corwin. Atomistic study of macroscopic analogs to short-chain molecules. *Physical Review E*, 91(2):022603, February 2015. doi: 10.1103/PhysRevE.91.022603. URL <http://link.aps.org/doi/10.1103/PhysRevE.91.022603>.
- [17] J. Clerk Maxwell. On the Dynamical Theory of Gases. *Philosophical Transactions of the Royal Society of London*, 157:49–88, January 1867. ISSN 0261-0523. URL <http://www.jstor.org/stable/108968>.
- [18] Joel L. Lebowitz. Statistical mechanics: A selective review of two central issues. *Reviews of Modern Physics*, 71(2):S346–S357, March 1999. doi: 10.1103/RevModPhys.71.S346. URL <http://link.aps.org/doi/10.1103/RevModPhys.71.S346>.
- [19] A. Einstein. Über die von der molekularkinetischen Theorie der Wärme geforderte Bewegung von in ruhenden Flüssigkeiten suspendierten Teilchen. *Annalen der Physik*, 322(8):549–560, 1905. ISSN 1521-3889. doi: 10.1002/andp.19053220806. URL <http://onlinelibrary.wiley.com/doi/10.1002/andp.19053220806/abstract>.
- [20] Jürgen Blum, Stefan Bruns, Daniel Rademacher, Annika Voss, Björn Willenberg, and Maya Krause. Measurement of the Translational and Rotational Brownian Motion of Individual Particles in a Rarefied Gas. *Physical Review Letters*, 97(23):230601, December 2006. doi: 10.1103/PhysRevLett.97.230601. URL <http://link.aps.org/doi/10.1103/PhysRevLett.97.230601>.
- [21] Tongcang Li, Simon Kheifets, David Medellin, and Mark G. Raizen. Measurement of the Instantaneous Velocity of a Brownian Particle. *Science*, 328(5986):1673–1675, June 2010. ISSN 0036-8075, 1095-9203. doi: 10.1126/science.1189403. URL <http://www.sciencemag.org/content/328/5986/1673>.
- [22] Rongxin Huang, Isaac Chavez, Katja M. Taute, Branimir Lukić, Sylvia Jeney, Mark G. Raizen, and Ernst-Ludwig Florin. Direct observation of the full transition from ballistic to diffusive Brownian motion in a liquid. *Nature Physics*, 7(7):576–580, July 2011. ISSN 1745-2473. doi: 10.1038/nphys1953. URL <http://www.nature.com/nphys/journal/v7/n7/full/nphys1953.html>.

- [23] Simon Kheifets, Akarsh Simha, Kevin Melin, Tongcang Li, and Mark G. Raizen. Observation of Brownian Motion in Liquids at Short Times: Instantaneous Velocity and Memory Loss. *Science*, 343(6178):1493–1496, March 2014. ISSN 0036-8075, 1095-9203. doi: 10.1126/science.1248091. URL <http://www.sciencemag.org/content/343/6178/1493>.
- [24] S. Douady. Experimental study of the Faraday instability. *Journal of Fluid Mechanics*, 221: 383–409, 1990. doi: 10.1017/S0022112090003603.
- [25] Wenbin Zhang and Jorge Viñals. Secondary Instabilities and Spatiotemporal Chaos in Parametric Surface Waves. *Physical Review Letters*, 74(5):690–693, January 1995. doi: 10.1103/PhysRevLett.74.690. URL <http://link.aps.org/doi/10.1103/PhysRevLett.74.690>.
- [26] R. Ramshankar, D. Berlin, and J. P. Gollub. Transport by capillary waves. Part I. Particle trajectories. *Physics of Fluids A: Fluid Dynamics (1989-1993)*, 2(11):1955–1965, November 1990. ISSN 0899-8213, 1089-7666. doi: 10.1063/1.857671. URL <http://scitation.aip.org/content/aip/journal/pofa/2/11/10.1063/1.857671>.
- [27] O. N. Mesquita, S. Kane, and J. P. Gollub. Transport by capillary waves: Fluctuating Stokes drift. *Physical Review A*, 45(6):3700–3705, March 1992. doi: 10.1103/PhysRevA.45.3700. URL <http://link.aps.org/doi/10.1103/PhysRevA.45.3700>.
- [28] Preben Alstrøm, Jacob Sparre Andersen, Walter I. Goldburg, and Mogens T. Levinsen. Relative diffusion in a chaotic system: Capillary waves in the Faraday experiment. *Chaos, Solitons & Fractals*, 5(8):1455–1464, August 1995. ISSN 0960-0779. doi: 10.1016/0960-0779(95)00024-X. URL <http://www.sciencedirect.com/science/article/pii/096007799500024X>.
- [29] Elsebeth Schröder, Jacob Sparre Andersen, Mogens T. Levinsen, Preben Alstrøm, and Walter I. Goldburg. Relative Particle Motion in Capillary Waves. *Physical Review Letters*, 76(25):4717–4720, June 1996. doi: 10.1103/PhysRevLett.76.4717. URL <http://link.aps.org/doi/10.1103/PhysRevLett.76.4717>.
- [30] Adam E. Hansen, Elsebeth Schröder, Preben Alstrøm, Jacob Sparre Andersen, and Mogens T. Levinsen. Fractal Particle Trajectories in Capillary Waves: Imprint of Wavelength. *Physical Review Letters*, 79(10):1845–1848, September 1997. doi: 10.1103/PhysRevLett.79.1845. URL <http://link.aps.org/doi/10.1103/PhysRevLett.79.1845>.
- [31] A. von Kameke, F. Huhn, G. Fernández-García, A. P. Muñozuri, and V. Pérez-Muñozuri. Double Cascade Turbulence and Richardson Dispersion in a Horizontal Fluid Flow Induced by Faraday Waves. *Physical Review Letters*, 107(7):074502, August 2011. doi: 10.1103/PhysRevLett.107.074502. URL <http://link.aps.org/doi/10.1103/PhysRevLett.107.074502>.
- [32] N. Tokugawa, M. Umeki, and T. Kambe. Statistical analysis of particle drifts on Faraday waves. *Fluid Dynamics Research*, 16(1):43–55, July 1995. ISSN 0169-5983. doi: 10.1016/0169-5983(94)00013-P. URL <http://www.sciencedirect.com/science/article/pii/016959839400013P>.
- [33] J. Casas-Vázquez and D. Jou. Temperature in non-equilibrium states: a review of open problems and current proposals. *Reports on Progress in Physics*, 66(11):1937, November 2003. ISSN 0034-4885. doi: 10.1088/0034-4885/66/11/R03. URL <http://iopscience.iop.org/0034-4885/66/11/R03>.

- [34] Chaoming Song, Ping Wang, and Hernán A. Makse. Experimental measurement of an effective temperature for jammed granular materials. *Proceedings of the National Academy of Sciences of the United States of America*, 102(7):2299–2304, February 2005. ISSN 0027-8424, 1091-6490. doi: 10.1073/pnas.0409911102. URL <http://www.pnas.org/content/102/7/2299>.
- [35] Yoshiki Hidaka, Yusaku Hosokawa, Noriko Oikawa, Koyo Tamura, Rinto Anugraha, and Shoichi Kai. A nonequilibrium temperature and fluctuation theorem for soft-mode turbulence. *Physica D: Nonlinear Phenomena*, 239(11):735–738, June 2010. ISSN 0167-2789. doi: 10.1016/j.physd.2009.07.003. URL <http://www.sciencedirect.com/science/article/pii/S0167278909002140>.
- [36] H. W. Müller, R. Friedrich, and D. Papathanassiou. Theoretical and Experimental Investigations of the Faraday Instability. In *Evolution of Spontaneous Structures in Dissipative Continuous Systems*, number 55 in Lecture Notes in Physics, pages 230–265. Springer Berlin Heidelberg, January 1998. ISBN 978-3-540-65154-3 978-3-540-49537-6.
- [37] F. Simonelli and J. P. Gollub. Surface wave mode interactions: effects of symmetry and degeneracy. *Journal of Fluid Mechanics*, 199:471–494, 1989. doi: 10.1017/S0022112089000443.
- [38] M. C. Cross and P. C. Hohenberg. Pattern formation outside of equilibrium. *Reviews of Modern Physics*, 65(3):851–1112, July 1993. doi: 10.1103/RevModPhys.65.851. URL <http://link.aps.org/doi/10.1103/RevModPhys.65.851>.
- [39] A. M. Rucklidge, M. Silber, and A. C. Skeldon. Three-Wave Interactions and Spatiotemporal Chaos. *Physical Review Letters*, 108(7):074504, February 2012. doi: 10.1103/PhysRevLett.108.074504. URL <http://link.aps.org/doi/10.1103/PhysRevLett.108.074504>.
- [40] Raghuveer Parthasarathy. Rapid, accurate particle tracking by calculation of radial symmetry centers. *Nature Methods*, 9(7):724–726, July 2012. ISSN 1548-7091. doi: 10.1038/nmeth.2071. URL <http://www.nature.com/nmeth/journal/v9/n7/abs/nmeth.2071.html>.
- [41] William Sutherland. The viscosity of gases and molecular force. *Philosophical Magazine Series 5*, 36(223):507–531, 1893. ISSN 1941-5982. doi: 10.1080/14786449308620508. URL <http://www.tandfonline.com/doi/abs/10.1080/14786449308620508>.
- [42] Volker Schaller, Christoph Weber, Christine Semmrich, Erwin Frey, and Andreas R. Bausch. Polar patterns of driven filaments. *Nature*, 467(7311):73–77, September 2010. ISSN 0028-0836. doi: 10.1038/nature09312. URL <http://www.nature.com/nature/journal/v467/n7311/full/nature09312.html>.
- [43] N. D. Mermin and H. Wagner. Absence of Ferromagnetism or Antiferromagnetism in One- or Two-Dimensional Isotropic Heisenberg Models. *Physical Review Letters*, 17(22):1133–1136, November 1966. doi: 10.1103/PhysRevLett.17.1133. URL <http://link.aps.org/doi/10.1103/PhysRevLett.17.1133>.
- [44] J. M. Kosterlitz and D. J. Thouless. Ordering, metastability and phase transitions in two-dimensional systems. *Journal of Physics C: Solid State Physics*, 6(7):1181, April 1973. ISSN 0022-3719. doi: 10.1088/0022-3719/6/7/010. URL <http://iopscience.iop.org/0022-3719/6/7/010>.

- [45] John Toner and Yuhai Tu. Long-Range Order in a Two-Dimensional Dynamical XY Model: How Birds Fly Together. *Physical Review Letters*, 75(23):4326–4329, December 1995. doi: 10.1103/PhysRevLett.75.4326. URL <http://link.aps.org/doi/10.1103/PhysRevLett.75.4326>.
- [46] Ornstein. On the Brownian Motion. *Proc. Acad. Amst.*, 21:96–108, 1919.
- [47] Furth. *Zeits. f. Physik*, 2:244, 1920.
- [48] Christian L. Vestergaard, Paul C. Blainey, and Henrik Flyvbjerg. Optimal estimation of diffusion coefficients from single-particle trajectories. *Physical Review E*, 89(2):022726, February 2014. doi: 10.1103/PhysRevE.89.022726. URL <http://link.aps.org/doi/10.1103/PhysRevE.89.022726>.
- [49] A. Wernet, C. Wagner, D. Papathanassiou, H. W. Müller, and K. Knorr. Amplitude measurements of Faraday waves. *Physical Review E*, 63(3):036305, February 2001. doi: 10.1103/PhysRevE.63.036305. URL <http://link.aps.org/doi/10.1103/PhysRevE.63.036305>.
- [50] R. P. Ojha, P.-A. Lemieux, P. K. Dixon, A. J. Liu, and D. J. Durian. Statistical mechanics of a gas-fluidized particle. *Nature*, 427(6974):521–523, February 2004. ISSN 0028-0836. doi: 10.1038/nature02294. URL <http://www.nature.com/nature/journal/v427/n6974/full/nature02294.html>.
- [51] George M. Whitesides and Bartosz Grzybowski. Self-assembly at all scales. *Science (New York, N.Y.)*, 295(5564):2418–2421, March 2002. ISSN 1095-9203. doi: 10.1126/science.1070821.
- [52] Simon Tricard, Efraim Feinstein, Robert F. Shepherd, Meital Reches, Phillip W. Snyder, Dileni C. Bandarage, Mara Prentiss, and George M. Whitesides. Analog modeling of Worm-Like Chain molecules using macroscopic beads-on-a-string. *Physical Chemistry Chemical Physics*, 14(25):9041–9046, June 2012. ISSN 1463-9084. doi: 10.1039/C2CP40593H. URL <http://pubs.rsc.org/en/content/articlelanding/2012/cp/c2cp40593h>.
- [53] Rebecca Cademartiri, Claudiu A. Stan, Vivian M. Tran, Evan Wu, Liam Friar, Daryl Vulis, Logan W. Clark, Simon Tricard, and George M. Whitesides. A simple two-dimensional model system to study electrostatic-self-assembly. *Soft Matter*, 8(38):9771–9791, September 2012. ISSN 1744-6848. doi: 10.1039/C2SM26192H. URL <http://pubs.rsc.org/en/content/articlelanding/2012/sm/c2sm26192h>.
- [54] L. J. Fetters, D. J. Lohse, D. Richter, T. A. Witten, and A. Zirkel. Connection between Polymer Molecular Weight, Density, Chain Dimensions, and Melt Viscoelastic Properties. *Macromolecules*, 27(17):4639–4647, August 1994. ISSN 0024-9297. doi: 10.1021/ma00095a001. URL <http://dx.doi.org/10.1021/ma00095a001>.
- [55] Reza Vafabakhsh and Taekjip Ha. Extreme Bendability of DNA Less than 100 Base Pairs Long Revealed by Single-Molecule Cyclization. *Science*, 337(6098):1097–1101, August 2012. ISSN 0036-8075, 1095-9203. doi: 10.1126/science.1224139. URL <http://www.sciencemag.org/content/337/6098/1097>.
- [56] Christopher J. Buchko, Loui C. Chen, Yu Shen, and David C. Martin. Processing and microstructural characterization of porous biocompatible protein polymer thin films. *Polymer*, 40(26):7397–7407, December 1999. ISSN 0032-3861. doi: 10.1016/S0032-3861(98)00866-0. URL <http://www.sciencedirect.com/science/article/pii/S0032386198008660>.

- [57] Jianyong Ouyang, Chih-Wei Chu, Charles R. Szmanda, Liping Ma, and Yang Yang. Programmable polymer thin film and non-volatile memory device. *Nature Materials*, 3(12): 918–922, December 2004. ISSN 1476-1122. doi: 10.1038/nmat1269. URL <http://www.nature.com/nmat/journal/v3/n12/abs/nmat1269.html>.
- [58] Erik Winfree, Furong Liu, Lisa A. Wenzler, and Nadrian C. Seeman. Design and self-assembly of two-dimensional DNA crystals. *Nature*, 394(6693):539–544, August 1998. ISSN 0028-0836. doi: 10.1038/28998. URL <http://www.nature.com/nature/journal/v394/n6693/full/394539a0.html>.
- [59] Paul W. K. Rothmund. Folding DNA to create nanoscale shapes and patterns. *Nature*, 440(7082):297–302, March 2006. ISSN 0028-0836. doi: 10.1038/nature04586. URL <http://www.nature.com/nature/journal/v440/n7082/full/nature04586.html>.
- [60] S. B. Smith, L. Finzi, and C. Bustamante. Direct mechanical measurements of the elasticity of single DNA molecules by using magnetic beads. *Science*, 258(5085):1122–1126, November 1992. ISSN 0036-8075, 1095-9203. doi: 10.1126/science.1439819. URL <http://www.sciencemag.org/content/258/5085/1122>.
- [61] Jan Domke and Manfred Radmacher. Measuring the Elastic Properties of Thin Polymer Films with the Atomic Force Microscope. *Langmuir*, 14(12):3320–3325, June 1998. ISSN 0743-7463. doi: 10.1021/la9713006. URL <http://dx.doi.org/10.1021/la9713006>.
- [62] Carlos Bustamante, Zev Bryant, and Steven B. Smith. Ten years of tension: single-molecule DNA mechanics. *Nature*, 421(6921):423–427, January 2003. ISSN 0028-0836. doi: 10.1038/nature01405. URL <http://www.nature.com/nature/journal/v421/n6921/full/nature01405.html>.
- [63] Gary S. Grest and Kurt Kremer. Molecular dynamics simulation for polymers in the presence of a heat bath. *Physical Review A*, 33(5):3628–3631, May 1986. doi: 10.1103/PhysRevA.33.3628. URL <http://link.aps.org/doi/10.1103/PhysRevA.33.3628>.
- [64] J. D. Honeycutt. A general simulation method for computing conformational properties of single polymer chains. *Computational and Theoretical Polymer Science*, 8(1–2):1–8, 1998. ISSN 1089-3156. doi: 10.1016/S1089-3156(97)00025-1. URL <http://www.sciencedirect.com/science/article/pii/S1089315697000251>.
- [65] Florian Müller-Plathe. Coarse-Graining in Polymer Simulation: From the Atomistic to the Mesoscopic Scale and Back. *ChemPhysChem*, 3(9):754–769, September 2002. ISSN 1439-7641. doi: 10.1002/1439-7641(20020916)3:9<754::AID-CPHC754>3.0.CO;2-U.
- [66] Dominik Fritz, Vagelis A. Harmandaris, Kurt Kremer, and Nico F. A. van der Vegt. Coarse-Grained Polymer Melts Based on Isolated Atomistic Chains: Simulation of Polystyrene of Different Tacticities. *Macromolecules*, 42(19):7579–7588, October 2009. ISSN 0024-9297. doi: 10.1021/ma901242h. URL <http://dx.doi.org/10.1021/ma901242h>.
- [67] E. Ben-Naim, Z. A. Daya, P. Vorobieff, and R. E. Ecke. Knots and Random Walks in Vibrated Granular Chains. *Physical Review Letters*, 86(8):1414–1417, February 2001. doi: 10.1103/PhysRevLett.86.1414. URL <http://link.aps.org/doi/10.1103/PhysRevLett.86.1414>.
- [68] Ling-Nan Zou, Xiang Cheng, Mark L. Rivers, Heinrich M. Jaeger, and Sidney R. Nagel. The Packing of Granular Polymer Chains. *Science*, 326(5951):408–410, October 2009. ISSN 0036-8075, 1095-9203. doi: 10.1126/science.1177114. URL <http://www.sciencemag.org/content/326/5951/408>.

- [69] Pierre-Gilles Gennes. *Scaling Concepts in Polymer Physics*. Cornell University Press, Ithaca, NY, November 1979. ISBN 978-0-8014-1203-5.
- [70] H. Jensenius and G. Zocchi. Measuring the Spring Constant of a Single Polymer Chain. *Physical Review Letters*, 79(25):5030–5033, December 1997. doi: 10.1103/PhysRevLett.79.5030. URL <http://link.aps.org/doi/10.1103/PhysRevLett.79.5030>.
- [71] Bertrand Duplantier and Hubert Saleur. Winding-Angle Distributions of Two-Dimensional Self-Avoiding Walks from Conformal Invariance. *Physical Review Letters*, 60(23):2343–2346, June 1988. doi: 10.1103/PhysRevLett.60.2343. URL <http://link.aps.org/doi/10.1103/PhysRevLett.60.2343>.
- [72] Paul J. Flory. The Configuration of Real Polymer Chains. *The Journal of Chemical Physics*, 17(3):303–310, March 1949. ISSN 0021-9606, 1089-7690. doi: 10.1063/1.1747243. URL <http://scitation.aip.org/content/aip/journal/jcp/17/3/10.1063/1.1747243>.
- [73] Paul J. Flory. *Principles of Polymer Chemistry*. Cornell University Press, 1953. ISBN 0-8014-0134-8.
- [74] Shafiqh Mehraeen, Bariz Sudhanshu, Elena F. Koslover, and Andrew J. Spakowitz. End-to-end distribution for a wormlike chain in arbitrary dimensions. *Physical Review E*, 77(6):061803, June 2008. doi: 10.1103/PhysRevE.77.061803. URL <http://link.aps.org/doi/10.1103/PhysRevE.77.061803>.
- [75] Jan Wilhelm and Erwin Frey. Radial Distribution Function of Semiflexible Polymers. *Physical Review Letters*, 77(12):2581–2584, September 1996. doi: 10.1103/PhysRevLett.77.2581. URL <http://link.aps.org/doi/10.1103/PhysRevLett.77.2581>.
- [76] Paul. J. Flory and M. Volkenstein. Statistical mechanics of chain molecules. *Biopolymers*, 8(5): 699–700, November 1969. ISSN 1097-0282. doi: 10.1002/bip.1969.360080514. URL <http://onlinelibrary.wiley.com/doi/10.1002/bip.1969.360080514/abstract>.
- [77] Wayne L. Mattice and Ulrich W. Suter. *Conformational Theory of Large Molecules: The Rotational Isomeric State Model in Macromolecular Systems*. Wiley-Interscience, New York, 1 edition edition, October 1994. ISBN 978-0-471-84338-2.
- [78] Dominic Vella and L. Mahadevan. The “Cheerios effect”. *American Journal of Physics*, 73(9): 817–825, 2005. doi: 10.1119/1.1898523. URL <http://link.aip.org/link/?AJP/73/817/1>.
- [79] He Yi, Xin-Yu Bao, Richard Tiberio, and H.-S. Philip Wong. A General Design Strategy for Block Copolymer Directed Self-Assembly Patterning of Integrated Circuits Contact Holes using an Alphabet Approach. *Nano Letters*, 15(2):805–812, February 2015. ISSN 1530-6984. doi: 10.1021/nl502172m. URL <http://dx.doi.org/10.1021/nl502172m>.
- [80] Bryan Wei, Mingjie Dai, and Peng Yin. Complex shapes self-assembled from single-stranded DNA tiles. *Nature*, 485(7400):623–626, May 2012. ISSN 0028-0836. doi: 10.1038/nature11075. URL <http://www.nature.com/nature/journal/v485/n7400/abs/nature11075.html>.
- [81] Arivazhagan Rajendran, Masayuki Endo, Yousuke Katsuda, Kumi Hidaka, and Hiroshi Sugiyama. Programmed Two-Dimensional Self-Assembly of Multiple DNA Origami Jigsaw Pieces. *ACS Nano*, 5(1):665–671, January 2011. ISSN 1936-0851. doi: 10.1021/nn1031627. URL <http://dx.doi.org/10.1021/nn1031627>.

- [82] Sara Jabbari-Farouji, Erika Eiser, Gerard H. Wegdam, and Daniel Bonn. Ageing dynamics of translational and rotational diffusion in a colloidal glass. *Journal of Physics: Condensed Matter*, 16(41):L471, 2004. ISSN 0953-8984. doi: 10.1088/0953-8984/16/41/L07. URL <http://stacks.iop.org/0953-8984/16/i=41/a=L07>.
- [83] Charles-Édouard Lecomte and Antoine Naert. Experimental study of energy transport between two granular gas thermostats. *Journal of Statistical Mechanics: Theory and Experiment*, 2014(11):P11004, 2014. ISSN 1742-5468. doi: 10.1088/1742-5468/2014/11/P11004. URL <http://stacks.iop.org/1742-5468/2014/i=11/a=P11004>.
- [84] Heinrich M. Jaeger, Sidney R. Nagel, and Robert P. Behringer. Granular solids, liquids, and gases. *Reviews of Modern Physics*, 68(4):1259–1273, October 1996. doi: 10.1103/RevModPhys.68.1259. URL <http://link.aps.org/doi/10.1103/RevModPhys.68.1259>.